CHAPTER V

RESULTS AND DISCUSSION

5.1 Kevlar™ Fiber Characterization

Table 5.1 shows the thermal and mechanical properties of Kevlar™ fiber utilized in this work. It was evaluated and compared with standard properties of the commercialized Kevlar29, reported in by Yang, 1993. The glass transition temperature of our Kevlar™ fiber with the value of 348°C was observed in the DSC analysis. This value was somewhat lower than that of the reported glass transition temperature of 375°C of the commercial fiber. The TGA curves at a heating rate of 20°C/min under nitrogen atmosphere showed the degradation temperature at 5% weight loss of the Kevlar™ of about 536°C. The gauge length between the sample clamps was set at 2.54 cm. with the 10% per min strain rate for tensile property evaluation of the filament. The tensile modulus of the Kevlar™ fiber was determined to be 67 GPa having 5.5 % elongation at break. These values were comparable to those of the commercial Kevlar29 having the reported tensile modulus of 70 GPa and 3.6 % elongation at break (Yang, 1993).

5.2 Neat Resin Characterization

5.2.1 Spectroscopic Investigation of the Molecular Structures

In this work, polyurethane (PU) prepolymer was synthesized by a reaction of polyether polyol (MW. 2000) with isophorone diisocyanate (IPDI). The basic structures of PU prepolymer were studied by FT-IR spectroscopic technique. The important functional groups of the PU prepolymer are N=C=O, C=O, CH_2 and CH_3 which were used to characterize the presence of the prepolymer in the polymerization reaction. In the spectra, the bond around 2280-2240 cm^{-1} was attributed to the N=C=O

stretching of isocyanate structure. The carbonyl absorption (C=O) indicated the reaction of the isocyanate group with the hydroxyl group of the polyol to form a urethane linkage in the prepolymer. The urethane's carbonyl signal is usually located at 1730-1700 cm^{-1} whereas several C-H stretching signals are located between 3000-2800 cm^{-1}. Figure 5.1 shows the FT-IR spectra of a mixture of the IPDI and the diol before and after their reaction. From the figure, spectrum (b) indicated that the C=O peak was appeared at 1715 cm^{-1} and the N=C=O peak at 2270 cm^{-1} was significantly decreased with the progress of the reaction to form the prepolymer. The urethane prepolymer was confirmed to be obtained after the two reactants reacted at 90°C for 120 minutes under N_2 purging which was the condition to render spectrum (b).

The reaction between benzoxazine monomer(BA) and urethane prepolymer (PU) could also be analyzed by FT-IR technique. Figure 5.2 shows the FT-IR spectra of the BA/PU alloy at a mass ratio of 70/30. Figure 5.2 (a) reveals the spectrum of the BA/PU prepolymer which presented the mixed fingerprints of both the benzoxazine resin and the urethane prepolymer i.e. peaks at 942 cm^{-1} (C-O-C stretching mode) and 1232 cm^{-1} (tri-substituted benzene) from the benzoxazine resin and that of 2270 cm^{-1} (N=C=O stretching) and 1715 cm^{-1} (C=O stretching) from the PU prepolymer. After being fully-cured, the oxazine ring is known to be opened by the breakage of a C-O bond of the monomer, which further reacted with the N=C=O group of the PU. The mechanism was previously proposed by Takeichi et al., 2000 and was also observed by Rimdusit, et al., 2005. Figure 5.2 (b) also exhibits the spectrum of BA/PU polymer alloys indicating the absence the absorption bond at 942 cm^{-1} (C-O-C bond) and at 2270 cm^{-1} (NCO group). These results are also in good agreement with the previous reports by Takeichi et al., 2000 and Rimdusit, et al., 2005

5.2.2 Curing Condition and Thermal Property Analysis of the Alloys

The curing exotherms of the neat benzoxazine resin (BA) and the binary mixtures between the benzoxazine and the urethane resin (BA/PU) were shown in Figure 5.3. The investigated compositions of the BA/PU mixtures were 60/40, 70/30, 80/20, 90/10 and 100/0 mass ratios. From this plot, the addition of the urethane resin

in the benzoxazine resin resulted in a shift of the curing peak maxima of the neat benzoxazine resin at 227°C to a higher temperature. The positions of the peaks ranging from about 235°C for BA/PU at 90/10 mass ratio to about 250°C for BA/PU at 60/40 mass ratio. In principle, the reactions between BA/PU were expected to comprise of at least two reactions; the first reaction is the exothermic curing peak among the benzoxazine monomers that shows the peak maximum centered at 227°C, while the second one is likely to be the reaction between the isocyanate group on the urethane monomer with the phenolic hydroxyl group on the polybenzoxazine. The reaction between the isocyante group with phenolic hydroxyl group on polybenzoxazine was expected to proceed after phenolic hydroxyl group from the ring opening of the benzoxazine monomer was produced. In addition, as the urethane prepolymer could not react to form a homopolymer by itself, its presence with an increasing amount might cause a dilution effect on the resulting BA/PU mixtures. As a consequence, the curing retardation was observed and was more pronounced with the increasing amount of the PU in the binary mixtures. The thermogram also shows the decrease of the area under the curves of the binary mixtures when the amount of the urethane resin increased. The phenomenon is attributed to the change from the BA/BA interaction to a more BA/PU interaction with increasing the PU fraction in the alloys. The systematic decrease of the exotherms with the PU implied that the BA/PU interaction possessed a lower heat of reaction per mole of the reactant compared to that of the BA/BA interaction. Excessive amount of the PU in the binary mixtures might also lead to the presence of the unreacted PU in the fully cured alloys. Our BA/PU alloys with the PU mass fraction of less than 30% was found to yield a fully cured system of an infinite network as confirmed by the solvent extraction test.

Figure 5.4 exhibits the DSC thermograms of the mixtures of the benzoxazine and urethane resins at a mass ratio of 60/40 at various curing conditions. The composition was selected to represent all alloys for determining the full cured condition as the ratio required the most thermal energy for curing. The heat of reaction determined from the area under the exothermic peak is 159.6 J/g for the uncured 60/40 BA/PU mixture. It was reduced to 100.2 J/g after curing at 160°C for 2 hrs and decreased to 36.9 J/g after further curing at 180°C for 2 hrs. Furthermore, after

post curing at 200°C for 2 hrs, the exothermic heat of reaction was found to be as low as 3.4 J/g corresponding to approximately 95% conversion. The degree of conversion of the sample was determined according to the following relationship:

$$\% \text{ conversion} = (1 - \frac{H_{rxn}}{H_o}) \times 100 \qquad (5.1)$$

where H_{rxn} is the heat of reaction of the partially cured specimens, whereas H_o is the heat of reaction of the uncured resin. Both quantities were determined from DSC experiments. The obtained curing conversion indicated that the curing reaction of the BA/PU polymer alloys could rapidly occur at higher temperature. Figure 5.5 suggested that the condition for complete curing of the benzoxazine alloys was 160°C for 2 hrs, 180°C for 2 hrs, and 200°C for 2 hrs as indicated by the disappearance of the area under the exothermic peak of more than 95%, in this case. Based on the above curing condition, the degree of conversions were determined to be 96% in BA/PU = 70/30, 98% in BA/PU = 80/20, >98% in BA/PU = 90/10, and >98% in the unmodified polybenzoxazine, respectively.

The effect of the urethane mass fraction on the glass transition temperature of the BA/PU polymer alloys was previously reported by Rimdusit, et al., 2005 using DMA. In these alloy systems, their glass transition temperatures showed a synergestic behavior as T_gs were observed to increase to the values greater than the T_gs of both parent polymers with the mass fraction of the PU. Figure 5.5 and Figure 5.6 show the DSC thermograms and the corresponding glass transition temperatures (T_gs) obtained from the thermograms of the fully cured BA/PU matrix alloys. The T_gs of these BA/PU binary systems were again found to increase with the mass fraction of the PU confirming our previous report (Rimdusit et al., 2005). The glass transition temperatures of the PU and the poly(BA-a) were reported to be about -70°C and 165°C, respectively. However, the glass transition temperature of the fully cured BA/PU alloys were observed to be 180°C in 90/10 BA/PU, 208°C in 80/20 BA/PU, 219°C in 70/30 BA/PU and 246°C in 60/40 BA/PU. The observed increase in the crosslink density of the binary systems with PU is one possible reason for the enhancement in the T_g of the resulting alloys though PU is a softer molecular species

having low T_g and was expected to lower the T_g of the binary alloys. The phenomenon was attributed to the additional crosslinking caused by the reaction between an isocyanate group on a urethane monomer with a hydroxyl group on polybenzoxazine after the phenolic hydroxyl group from the ring opening of benzoxazine monomer was produced (Rimdusit et al., 2005).

5.2.3 Thermal Degradation Behaviors of the BA/PU Alloys

Figure 5.7 showed a TGA profile of the polybenzoxazine and BA/PU alloys at various compositions. Normally, degradation temperature (T_d) e.g. at 5% weight loss, is one of the key parameters needed to be considered for high temperature applications. Our results revealed that the degradation temperatures of the polymer alloys were slightly higher than that of the polybenzoxazine homopolymer. The degradation temperature of the pure polybenzoxazine at 5%wt loss was determined to be 315°C whereas the decomposition temperatures of the BA/PU polymer alloys were approximately 326°C. These results might be due to the reaction of the isocyanate of the urethane prepolymer and the hydroxyl of the polybenzoxazine helped increase a crosslink density of the polymer alloys as explained earlier. Therefore, one benefit of incorporating the PU into the BA network was to improve the thermal stability of the polybenzoxazine as a result of crosslinking density enhancement. In addition, the residual weight at 800°C of the binary systems was found to decrease with increasing the PU fraction in the alloys. The char yield at 800°C of the polybenzoxazine was determined to be 25 wt% which was consistent with the value reported by Takeichi and Guo, 2000. The IPDI-polyol based polyurethane possessed a lower char yield of only 23 wt% even at a higher temperature of 600°C (Mallakpour and Isfakani, 2002). The increase of the PU fractions was thus expectedly to decrease the char yield of the alloys as observed in Figure 5.7. This can be explained as the structure of the polybenzoxazine contained a more thermally stable benzene rings compared to the mostly aliphatic structure of the diol in the urethane. Consequently, the addition of the urethane resulted in the lowering of the char yield in the polymer alloys.

5.3 Composite Characterizations

5.3.1 Curing Condition Determination

Figure 5.8 illustrates the DSC thermogram of Kevlar™-reinforced 60/40 BA/PU alloy prepregs. When comparing Figure 5.8 with Figure 5.3, the thermograms of our prepregs possessed curing exotherms with the same peak maxima as that of the 60/40 BA/PU resin. This characteristic indicated that the Kevlar™ fiber used had no effect on the curing reaction either retarding or accelerating the curing reaction of the matrix resin. In other words, the fiber is chemically inert to the benzoxazine curing reaction.

From Figure 5.8, the processing condition of the Kevlar™-BA/PU prepregs was thus chosen to be the same as that of the unreinforced resins i.e. at 160°C for 2 hrs, 180°C for 2 hrs, and 200°C for 2 hrs. The condition was also selected to ensure that the fully cured stage was obtained in every tested BA/PU mixture. The complete polymerization of the composites was obtained as indicated by the disappearance of the curing exotherms in DSC analyses. In addition, this condition was moderate enough for the Kevlar™ fiber which will degrade at above 536°C. The above condition was; therefore, used to cure our polymer alloys and their Kevlar™-reinforced composite prepregs.

5.3.2 Composition Determination of the Composites.

From the TGA thermograms of the unfilled polymer alloys and their composites in Figure 5.7 and Figure 5.9, the percent matrix content could be estimated. The mass fraction of the matrices of the composites determined from the thermograms using a relatively large sample mass of 25-30 mg were calculated to be approximately 20% in BA/PU = 60/40, 20% in BA/PU = 80/20, and 18% in BA/PU = 100/0 respectively. The fiber content was thus about the same for all composites using the same hot-pressing condition. The content was also in the optimal range for

producing composite armors as suggested by Park, 1996, 1999. This composition of the Kevlar™ fiber was fixed for all composites produced in this work.

5.3.3 Thermal Stability Investigation

From Figure 5.9, the degradation temperatures at 5 wt% loss of Kevlar™-reinforced benzoxazine alloy composites were, again, found to decrease systematically with increasing the mass fraction of the PU in the alloys. The degradation temperatures at 5% weight loss of the Kevlar™-reinforced benzoxazine alloys with the PU compositions of 0 to 40 % by weight was ranging from 374°C to 329°C. Another important feature in the thermograms is the weight residue at 800°C or the char yield of the composites which is related to the flammability of materials and is essential for some ballistic armor applications. The char yield was found to systematically reduce from 44.5% to 35.6% with an incorporation of the PU from 0 to 40% by weight. In addition, However, the values were all greater than those of the matrix alloys comparing at the same PU content. This is due to the fact that the char yields of the composites also included the additional residue of the Kevlar™ fiber which possessed a char yield of 44% i.e. at 600°C (Yang, 1993).

5.3.4 Mechanical Property Evaluation of the Composite Armor

Flexural properties of the Kevlar™-reinforced polybenzoxazine alloys were depicted in Figures 5.10 and 5.11. From Figure 5.10, flexural strengths of the Kevlar™ composites at various urethane mass fractions possessed the maximum value of 163 MPa in 100/0 BA/PU and systematically decreased to 52 MPa when using 60/40 BA/PU alloy as a matrix. We also observed the strengths of the composites to decrease in a linear manner with the composition of the PU in the matrix alloys. In addition, flexural moduli of the composites were found to significantly decrease with increasing the amount of the PU in the alloys from 18.3 GPa at 0% by weight of PU to about 7.5 GPa at 40% by weight of PU as illustrated in Figure 5.11. The phenomenon was due to the fact that the addition of the rubbery urethane polymer into the adamantine polybenzoxazine was able to lower either the

strength or the stiffness of the resulting polybenzoxazine alloys as clearly seen in both figures.

5.3.5 Dynamic Mechanical Property Investigation of the Composites

The dynamic mechanical properties of the BA/PU matrix alloys and the Kevlar^{TM}-reinforced BA/PU are shown in Figures 5.12-5.16. From Figure 5.12, the storage moduli in the glassy state of the BA/PU alloys expectedly decreased when the PU fraction increased as a result of the incorporation of the more flexible PU structure in the alloys as already described in the previous section. At room temperature, the storage moduli of the BA/PU polymer alloys were systematically reduced from 5.7 GPa to 1.4 GPa with the addition of the PU from 0 to 40% by weight. The values are about the same of those reported previously (Rimdusit et al., 2005). In addition, the modulus in the rubbery plateau moduli tended to increase with the mass fraction of the PU. This suggested that the increase in the PU content in the polymer alloys possibly resulted in an enhancement of the crosslink density of the fully cured specimens. In Figure 5.14, the storage moduli of Kevlar^{TM}-reinforced benzoxazine alloys in the same compositional range of 0 to 40 % by weight of the PU were ranging from 16.4 GPa to 2.8 GPa.

Glass transition temperatures of the composites were also detected in the dynamic mechanical thermograms based on the maxima of their loss moduli, G". The T_g values of the BA/PU polymer alloys were found to increase with increasing the amount of the PU fraction as also observed in the DSC experiments. According to Figure 5.14, a higher crosslink density of the matrix alloys as in indicated by a higher plateau modulus with increasing the amount of the PU led to a higher T_g of the matrix. The effect of a crosslink density on a T_g of the polymer network can be accounted for using Fox and Loshaek equation:

$$Tg = Tg(\infty) - \frac{k}{M_n} + k_x \rho \qquad (5.3)$$

where $Tg(\infty)$ is the T_g of infinite molecular weight linear polymer, k and k_x are the numerical constants, M_n is the number averaged molecular weight and ρ is the crosslink density respectively.

From Figure 5.17, T_gs of our Kevlar-reinforced composites exhibited the values significantly higher than those of the neat BA/PU matrices comparing at the same mass fraction of the PU in the alloys. The implication of these phenomena is probably due to the contribution of the substantial interfacial adhesion between the Kevlar^{TM} fiber and the polybenzoxazine alloys.

The α-relaxation peaks of the loss factor or tan δ of composites are shown in Figure 5.18. The magnitude of tan δ was observed to decrease with the increasing mass fraction of the PU resin in the alloy matrices and the peak maxima also shifted to higher temperature. The magnitude at the temperature below T_g of the tan δ, was found to increase as the urethane content in the matrix was increased implying the more viscous characteristics of the alloys with the PU at low temperature. However, the peak height of the tanδ in the vicinity of T_g was observed to be smaller with the PU content. Since tanδ is a ratio of a viscous to an elastic component of dynamic moduli of a specimen, it can be surmised that its decreasing height with the PU around T_g is associated with a lower segmental mobility, and thus is indicative of a higher degree of crosslinking for the urethane-rich samples as observed in our BA/PU alloy systems. In other words, the polymer alloys are softer at room temperature due to the PU fraction but possess higher degree of crosslinking that can inhibit the large scale mobility at elevated temperature.

5.3.6 Firing Tests of the BA/PU Composite Armors

5.3.6.1 Specimen characterization

A series of ballistic tests were performed on the composite laminates which were made of Kevlar^{TM} fabric impregnated with BA/PU resins and cured using

the curing condition as suggested in the previous section. The Kevlar™ fabric used has the areal density of about 0.016 g/cm^2. The dimension of the laminated specimens was 25.4 mm×25.4 mm×1.8 mm, corresponding to ten plies of the Kevlar™ cloth impregnated with about 20 by weight of the resin mixtures as determined in section 5.3.2. In addition, the densities of the composites were determined to be 1.26 g/cm^3 in BA/PU = 60/40, 1.28 g/cm^3 in BA/PU = 70/30, 1.29 g/cm^3 in BA/PU = 80/20, 1.30 g/cm^3 in BA/PU = 90/10 and 1.31 g/cm^3 in BA/PU = 100/0.

5.3.6.2 Low level ballistic impact test

The composite laminates fabricated with a thickness of 10 plies of the Kevlar™ at various the BA/PU alloy compositions mentioned above were tested using a 9 mm handgun with standard lead projectiles having lead outer-coating. From the test results, the composite consisted of only 10 piles of Kevlar™ could not protect ballistic impact from the above projectiles. Therefore the 20 piles of Kevlar™ panels i.e. 10/10 panel arrangement, at all BA/PU alloy compositions were selected for the following tests. In addition, the bisphenol A-based epoxy-Kelar™ composites (i.e. cured by amine hardener) at the same fiber content were also used to compare its ballistic impact performance with our BA/PU matrix alloys. All the ballistic test results were tabulated in Table 5.3.

In Table 5.3, the ballistic test results of the 20-ply Kevlar™-reinforced BA/PU as well as epoxy composites are listed. Comparing the ballistic performance of the polybenzoxazine and the epoxy composites, though both composites with the 10/10 configuration of the composite panels could not resist the projectiles in this test, the polybenzoxazine composite panel exhibited obvious improvement in the energy absorption characteristics. The improvement was clearly observed from the greater delaminated area of the polybenzoxazine composites compared to the much smaller delaminated area of the epoxy composites as depicted in Figure 5.18a-b. The firing results also indicated that the 90/10 and the 80/20 mass ratios of the BA/PU matrix exhibited ballistic penetration resistance in comparison with the other compositions of the BA/PU alloys as well as the epoxy matrix i.e. Figures 5.18c-d. However, only the

composite from the 80/20 BA/PU matrix exhibited 100% ballistic penetration resistance. In Figure 5.18c, the ballistic impact performance of the Kevlar™-reinforced 80/20 BA/PU alloys revealed relatively larger delaminated area than those of the epoxy and the BA matrix. The delaminated area has been known to be one major component of the energy absorption mechanisms in ballistic impact. Further increase the PU mass fractions to 30% and 40% by weight in the composite matrices resulted in a poor ballistic impact resistance as noted in Table 5.3. This confirms the necessity of identifying optimal fiber-matrix interactions in order to yield a composite system of outstanding ballistic performance. The variation in the BA/PU alloy compositions allowing an optimal interaction between the alloy matrix and its reinforcing fiber was attributed to the outstanding ballistic performance obtained.

Important kinetic energy absorption of composite material composes of several mechanisms, including tensile failure of fibers, elastic deformation of composite, interlayer delamination, shear between layers in the composite, and inertia effect. Kinetic energy absorption may be attributed according to basic factors such as mechanical properties of the composite's constituents direction of fiber arrangement, as well as interfacial strength (Thornton, 2001; Morye et al., 2000). Fracture morphology of the composite specimen is sometimes used to qualitatively evaluate the possible kinetic energy absorption of the material. The SEM micrograph of the fracture morphology of Kevlar™ fiber is illustrated in Figure 5.21. The typical Kevlar™ fiber fractures were spilts along fiber direction and skin off. These damage fractures are consistent with the fiber damage previous reported by Sohn, et al., 2000. In their report, the scanning electron micrographs were used to observe impact fractures and damage mode at the fracture surfaces of the Kevlar™-laminated specimens comparing with those of Nylon fiber. In the study, the Nylon fiber exhibited no potential for resistance to ballistic impact and exhibited energy absorption to be significantly lower than of that the Kevlar™. The commonly observed fracture characteristics of Nylon fiber were broken fibers and fused end of the fiber line after impact with a 17-grain fragment simulator (Laible, Figucia and Ferguson, 1973).

The fracture surface of Kevlar™-reinforced BA/PU alloys at various compositions of PU is depicted in Figure 5.20a-d. In Figure 5.20a and b, the fracture surfaces near the center of ballistic impact of the Kevlar™- reinforced 80/20 BA/PU alloy exhibited substantial level of adhesive failure in which the fibers were largely stripped off the matrix materials with only small fragments of the matrix remained adhere to the fibers. This fracture phenomenon could be clearly distinguished from that of the 60/40 BA/PU composites, which showed much lower degree of interfacial failure. The weaker mechanical properties due to the excessive presence of the soft PU component might be one reason of the observed predominantly cohesive failure in this composite. In other case, the too strong adhesion between the Kevlar™ fibers and the BA/PU matrix alloy might be attributed to the poor ballistic performance of the matrix resulting in the low degree of composite delamination mechanism. These results also confirmed the effect of the BA/PU alloy compositions on the interaction between the Kevlar™ fibers and the alloy matrices and thus the ballistic performance of obtained polymer composites.

Consequently, the selection of a suitable matrix resin that renders the most energy absorption characteristics with particular reinforcing fiber used is crucial to the successful ballistic performance of the composite armor. The behaviors were also explained and discussed partly by Laible and Figucia, 1973 who studied the used of high-modulus organic fiber in three different types of matrix resins i.e. epoxy, phenolic, and polycarbonate. Each of the resin had reported to possess different protective levels i.e. epoxy had V_{50} = 649 ft/sec, phenolic provided V_{50} = 511 ft/sec, and polycarbonate gave V_{50} = 491 ft/sec. Last but not least, it should be noted that the BA resin seemed to render a synergistic behavior in ballistic performance with the PU system used with the 80/20 BA/PU rendering the most outstanding ballistic performance. The 80/20 BA/PU alloy was; therefore, further used to fabricate the composite armors for higher protection level evaluation.

5.3.6.3 Ballistic impact test of NIJ level II-A

The ballistic impact velocities required by NIJ standard for level II-A was used to study the effect of the composite panel thickness and arrangement based on the Kevlar^{TM}-reinforced 80/20 BA/PU alloys. Our composite samples were approximately 1.8 mm in thickness of 10 piles/panel, 3.5 mm and 5 mm in thickness of 20 piles/panel and 30 piles/panel composites respectively. The areal densities of the composites were determined to be 0.24 g/cm^2 in the 10 piles/panel composites, 0.48 g/cm^2 in the 20 piles/panel composites and 0.70 g/cm^2 in the 30 piles/panel composites. The Kevlar^{TM}-reinforced 80/20 BA/PU composite samples with 20 piles, and 30 piles thick were tested in this NIJ standard. The 20 ply composites were arranged in 2 patterns i.e. 10/10 configuration and 20/0 configuration. While the 30 ply composites were arranged in 3 patterns i.e. 10/10/10 configuration, 20/10/0 configuration, and 30/0/0 configuration

The results obtained for the NIJ level II-A ballistic test are shown in Table 5.4. All samples were fired with a 9 mm handgun, which, in practice, was known to have a greater impact velocity than that required by the NIJ standard of level II-A. The rear-side damage area of each sample was measured. In Table 5.4, the individual value for the deformed depth as well as the averaged diameter of the damaged area of the BA/PU composites after impacted with the projectiles was reported. From the table, all composite laminates assembled to have a combined thickness of 20 plies of the Kevlar^{TM} did not pass this level of the NIJ standard for ballistic protection. As a result, the 30-ply composite arrangements were evaluated. As seen in Table 5.4 and Figure 5.21, none of these 30-ply thick samples was perforated by the level II-A projectiles. From the delaminated area measurement, it is apparent that a sample with an arrangement of the 20-ply panel in front of the 10-ply panel (sample 2d) exhibited the best ballistic performance. The damaged area of this sample arrangement was significantly smaller than those of the other two arrangements i.e. the 10/10/10 configuration and 30/0/0 configuration. Therefore, the arrangement of composite panel in the firing test was found to be one important factor on the ballistic performance of the composites. The sample 2d had consisted of 20

plies panel in front of the 10 plies panel. The front panel with at least 20 plies of Kevlar^{TM} cloth was thus necessary for the level II-A resistance of perforation and was supposed to possess sufficient properties to destroy or deform this type of projectile. As a result, the kinetic energy was substantially reduced before piecing through the rear plate of 10 piles thick. Moreover, the energy might also be dissipated via the inertia effect when the projectile passed through the gap between the two plates. However, the front plate of sample 2c was found to possess insufficient mechanical integrity to destroy the projectiles. Consequently, a relatively large portion of the impact energy could still be transferred to the adjacent plate and caused relatively large damaged area to the rear plate. In the other hand, although, sample 2e possessed relatively high stiffness i.e. 30 plies in thickness, enough to substantially deform the projectile, this sample lacked the energy dissipation by an inertia effect as likely to occur in the 20/10 configuration. As a result, a larger damaged area comparing with sample 2d was observed. The cross-sections of the front plate of the tested composites with 20/10/0 and 30/0/0 arrangements are also illustrated in Figure 5.22 revealing the the macroscopic delamination of the Kevlar^{TM}'s cloth in the 20 plies and 30 plies thick composites. The picture might also be useful to roughly determine the size of the delamination of the tested composite specimens.

5.3.6.4 Ballistic impact test of level III-A

In this investigation, the Kevlar^{TM}-reinforced 80/20 BA/PU composite samples with the combined thickness of 40 piles, 50 piles, and 60 piles were subjected to a ballistic impact evaluation at a projectile velocity required by NIJ standard for level III-A. This III-A level test is currently the reported maximum level of protection based on polymer composites. The samples with the combined thickness of 40 plies had one type of arrangement, i.e. 20/10/10 configuration whereas the samples with the combined thickness of 50 plies had two types of arrangements, i.e. 30/20/0 configuration i.e. sample 3b, and 10/10/30 configuration i.e. sample 3c. In the case of composite samples with the combined thickness of 60 plies, the arrangements were set to be 30/20/10/0 configuration in sample 3d and 30/10/10/10 configuration in sample 3e. The test outcomes are listed in Table 5.5. Figure 5.23 also shows of the

photographs of some composites tested in this protection level revealing the damaged or delaminated areas of the samples.

From Table 5.5, it is apparent that the test weapon with standard 124 grains round lead projectile with a copper outer coating (Full Metal Jacket) typically used in the 9 mm handgun having a speed required by level III-A could be stopped with at least 50 plies of the composite samples. The damage area evaluation confirmed that the arrangement of composite panels had an important effect on their ballistic protection. It can be seen that sample 3b with 30/20 arrangement rendered the ballistically damaged depths and diameters smaller than those of sample 3c of the 10/10/30 arrangement. This result implied that the sample arrangement for level III-A protection needed at least 30-ply composite panel as a front plate in the impact direction. The sufficiently stiff panel seemed to play a crucial role as to deform the shape of the projectile as discussed previously. Figure 5.24 also depicts the side-view damage of sample 3b and 3c which again revealed significantly different levels of deformation due to different composite panel arrangements. .

In the combined 60-ply thick composite panels, the arrangement was set to be 30/20/10 configuration in sample 3d and 30/10/10/10 configuration in sample 3e. These two types of arrangements were again found to lead to different damaged areas and deformed depths. Sample 3e rendered less damaged area than sample 3d. Since the number of the Kevlar^{TM} plies combined was the same in each tested sample, the sample arrangement with the thicker panel of 30 piles for level III-A to be on the front and was found to be essential in the successful ballistic impact resistance of the composites with lower degree of sample deformations..

Table 5.1: Thermal and mechanical properties of the Kevlar^{TM}-fabric used.

Properties	**KevlarTM Used**	**Kevlar 29***
Diameter (μm)	12	12
Glass transition temperature(^{o}C)	348	375
Degradation temperature at 5% wt loss (^{o}C)	536	475
Char yield at 700 ^{o}C (%)	44	49
Modulus (GPa)	67	70
Elongation %	5.53	3.6

* Ref.:Yang, H.H. *Handbook of Kevlar aramid fiber*; John Wiley & Sons Ltd.; west Sussex, England, 1993.

Table 5.2: Density of Kevlar^{TM}-reinforced BA/PU composites at various PU contents.

PU Mass Fraction	Theoretical Density (g/cm^3)	Actual Density (g/cm^3)
0	1.37	1.31 ±0.004
0.1	1.36	1.30 ±0.012
0.2	1.35	1.29 ±0.007
0.3	1.35	1.28 ±0.004
0.4	1.34	1.26 ±0.008

Table 5.3: Effect of BA/PU alloy compositions on ballistic impact resistance using standard lead projectiles with lead outer coating typically used in 9 mm hand gun.

Number	Type of Matrix	Number of Plies Plate1+Plate2	Resistance to Penetration	
			Plate1	Plate2
1.1a	Epoxy	10+10	No	No
1.1b	Epoxy	10+10	No	No
1.2a	100/0 BA/PU	10+10	No	No
1.2b	100/0 BA/PU	10+10	No	No
1.3a	90/10 BA/PU	10+10	No	No
1.3b	90/10 BA/PU	10+10	Yes	Yes
1.4a	80/20 BA/PU	10+10	Yes	Yes
1.4b	80/20 BA/PU	10+10	Yes	Yes
1.5a	70/30 BA/PU	10+10	No	No
1.5b	70/30 BA/PU	10+10	No	No
1.6a	60/40 BA/PU	10+10	No	No
1.6b	60/40 BA/PU	10+10	No	No

Note: BA = polybenzoxazine

PU = urethane elastomer

Table 5.4: Effect of number of piles and panel arrangement of Kevlar^{TM}-reinforced 80/20 BA/PU composites after ballistic impact at projectiles velocities required by NIJ standard level II-A.

Sample Number	Number of Layers of Composites	Resistance to Penetration	Damage Dimension of the Rear Plate	
			Depth (mm)	Diameter (mm)
2a	10/10	No	-	-
2b	20/0	No	-	-
2c	10/10/10	Yes	10.8	69.5
2d	20/10/0	Yes	7.8	44.5
2e	30/0/0	Yes	8.7	66.6

Table 5.5: Effect of number of piles and panel arrangement of Kevlar^{TM} reinforced 80/20 BA/PU composites after ballistic impact at projectiles velocities required by NIJ standard level III-A.

Sample Number	Number of Layers of Composites	Impact Velosity (m/s)	Resistance to Penetration	Damage Dimension of the Rear Plate	
				Depth (mm)	Diameter (mm)
3a	20+10+10	426	No	-	-
3b	30+20	430	Yes	13.6	93.3
3c	10+10+30	429	Yes	19.5	119.1
3d	30+20+10	429	Yes	11.0	90.3
3e	30+10+10+10	431	Yes	10.1	66.1

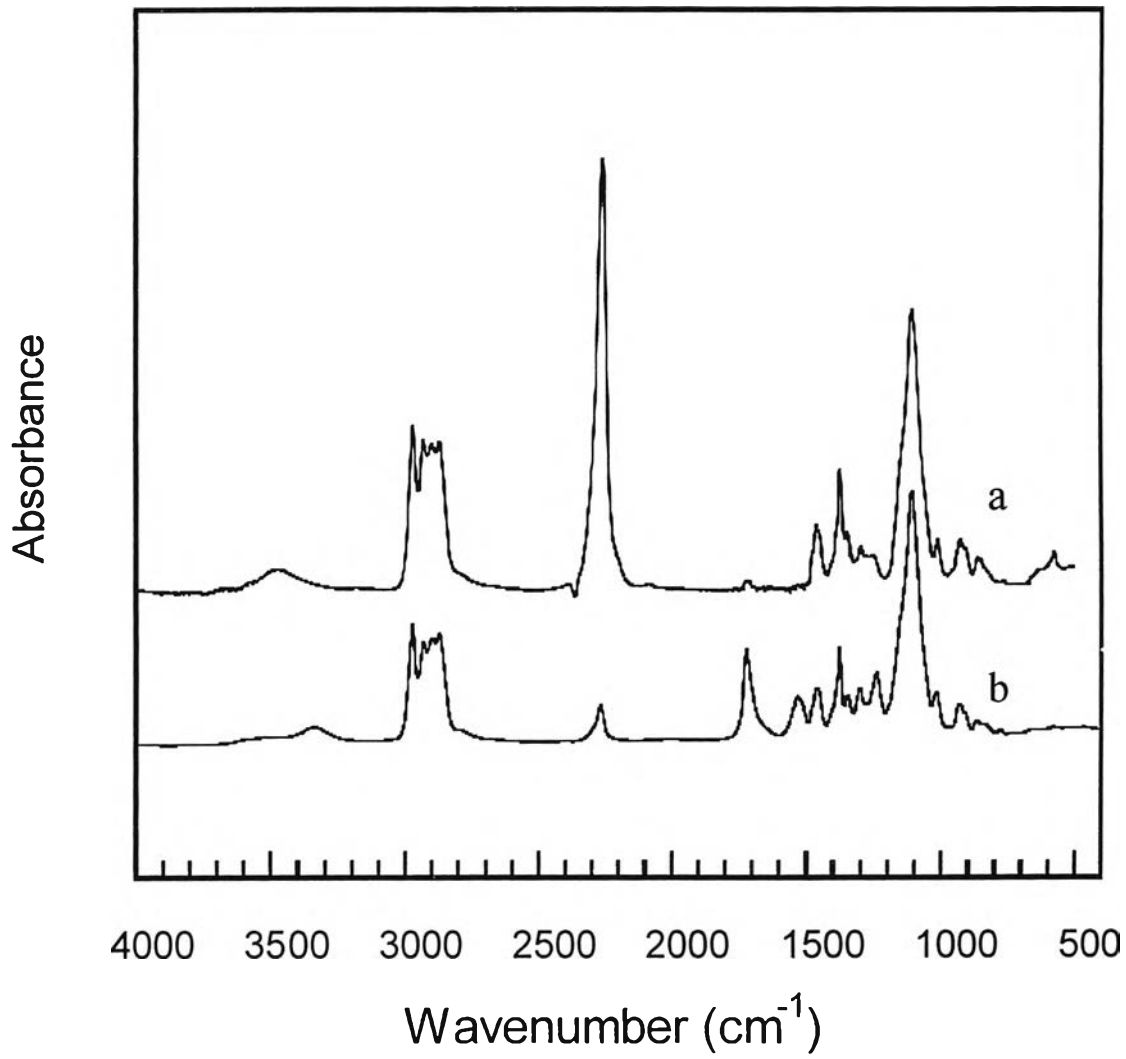

Figure 5.1: FT-IR Spectra of polyurethane prepolymer:
(a) IPDI+Diol mixture before synthesis, (b) IPDI+Diol prepolymer.

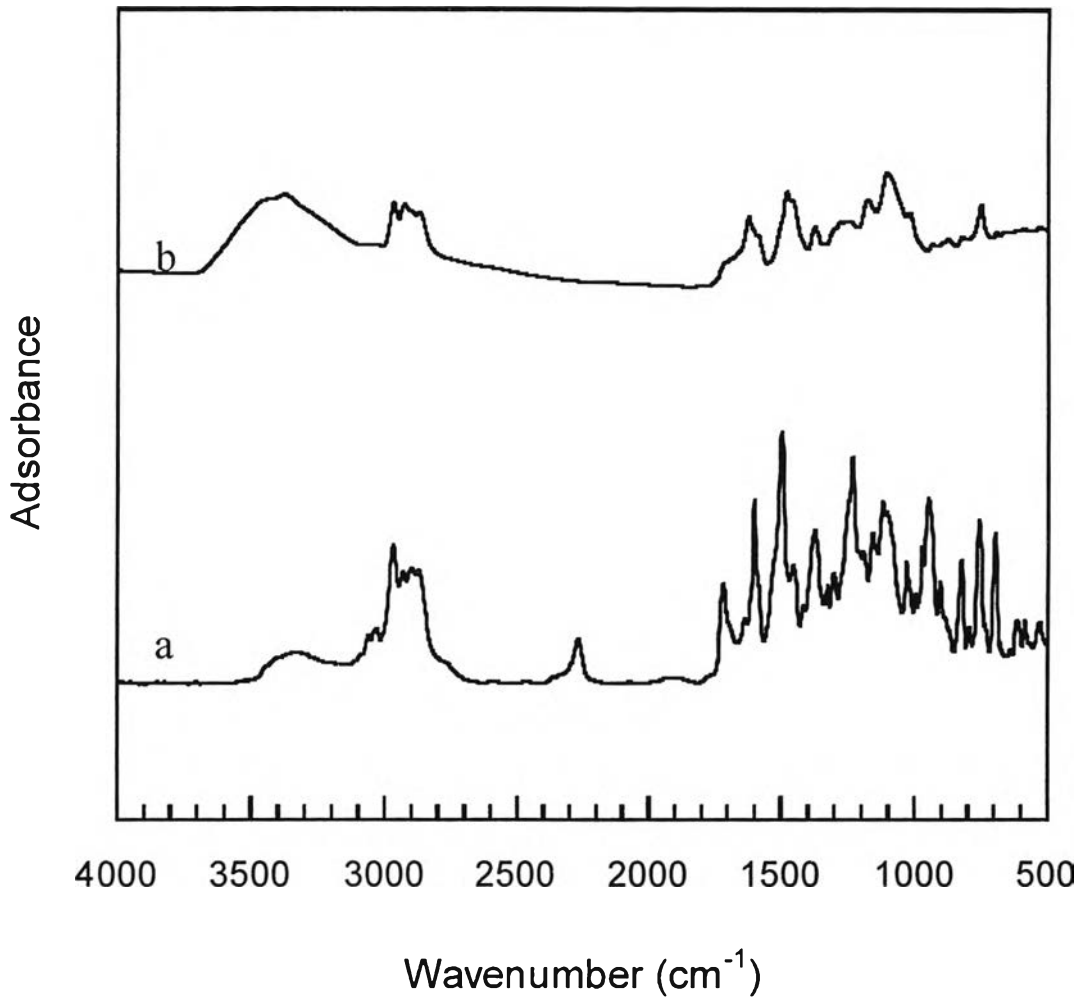

Figure 5.2: FT-IR Spectra of BA/PU alloy formation : (a)BA/PU 70/30 before curing, (b) BA/PU 70/30 after being fully cured at 160°C/2h, 170°C/1h, 180°C/2h,and 200°C/2h

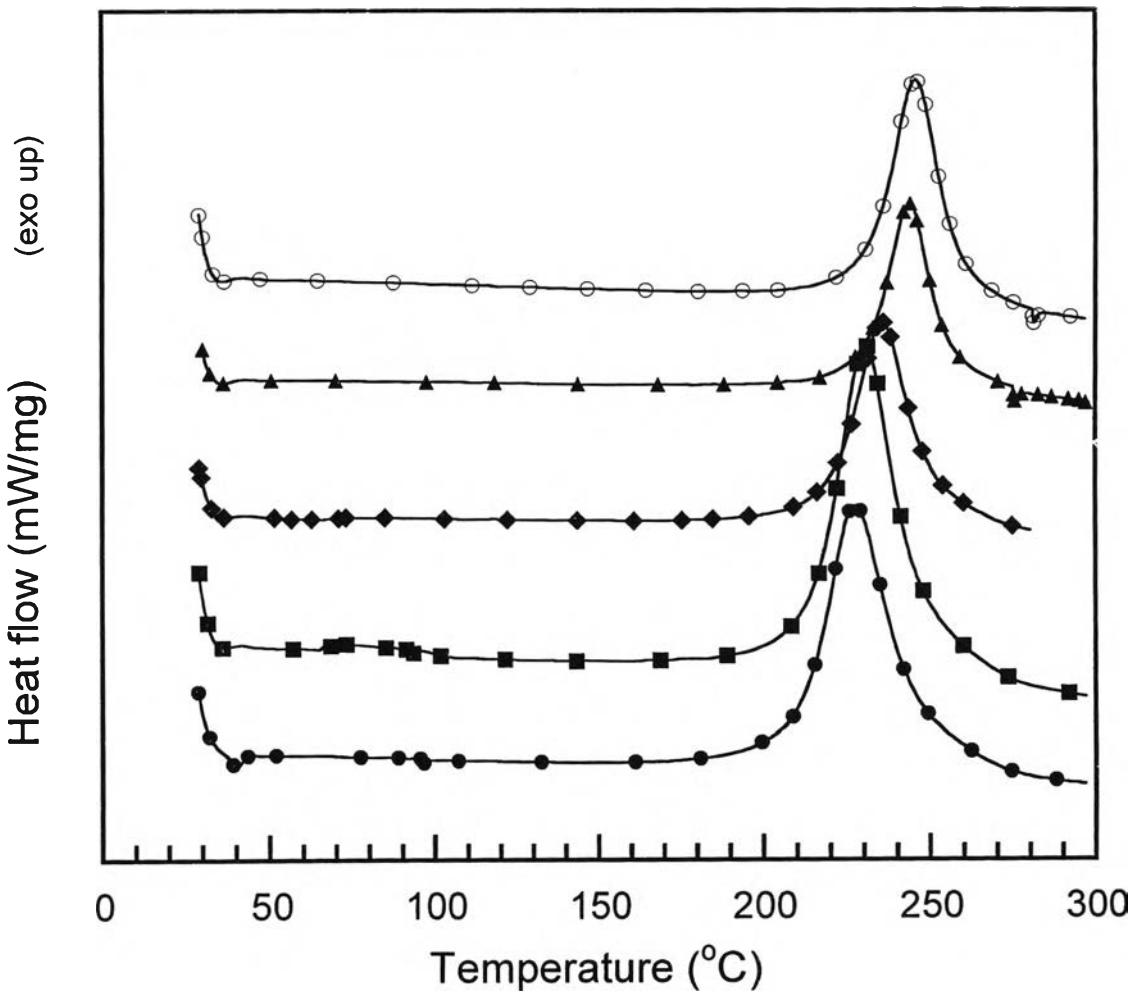

Figure 5.3: DSC thermograms of BA/PU resin mixture at various mass ratio : (●) 100/0, (■) 90/10, (◆) 80/20, (▲) 70/30, (○) 60/40

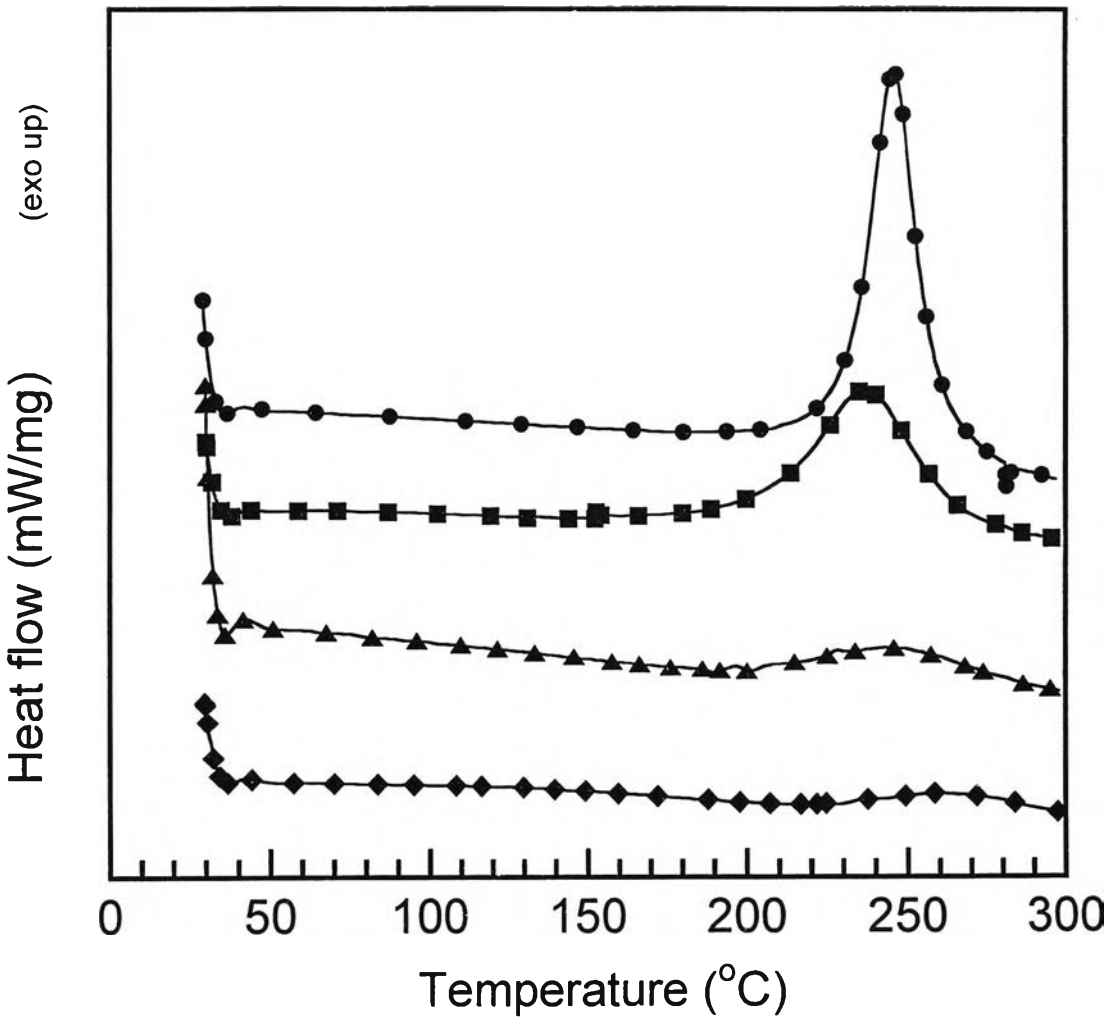

Figure 5.4: DSC thermograms of BA/PU at the mass ratio of 60/40 at various curing conditions: (●) uncured, (■) 160°C/2h, (◆) 160°C/2h,170°C/1h, and 180°C/2h, (▲) 160°C/2h, 170°C/1h, 180°C/2h,and 200°C/2h

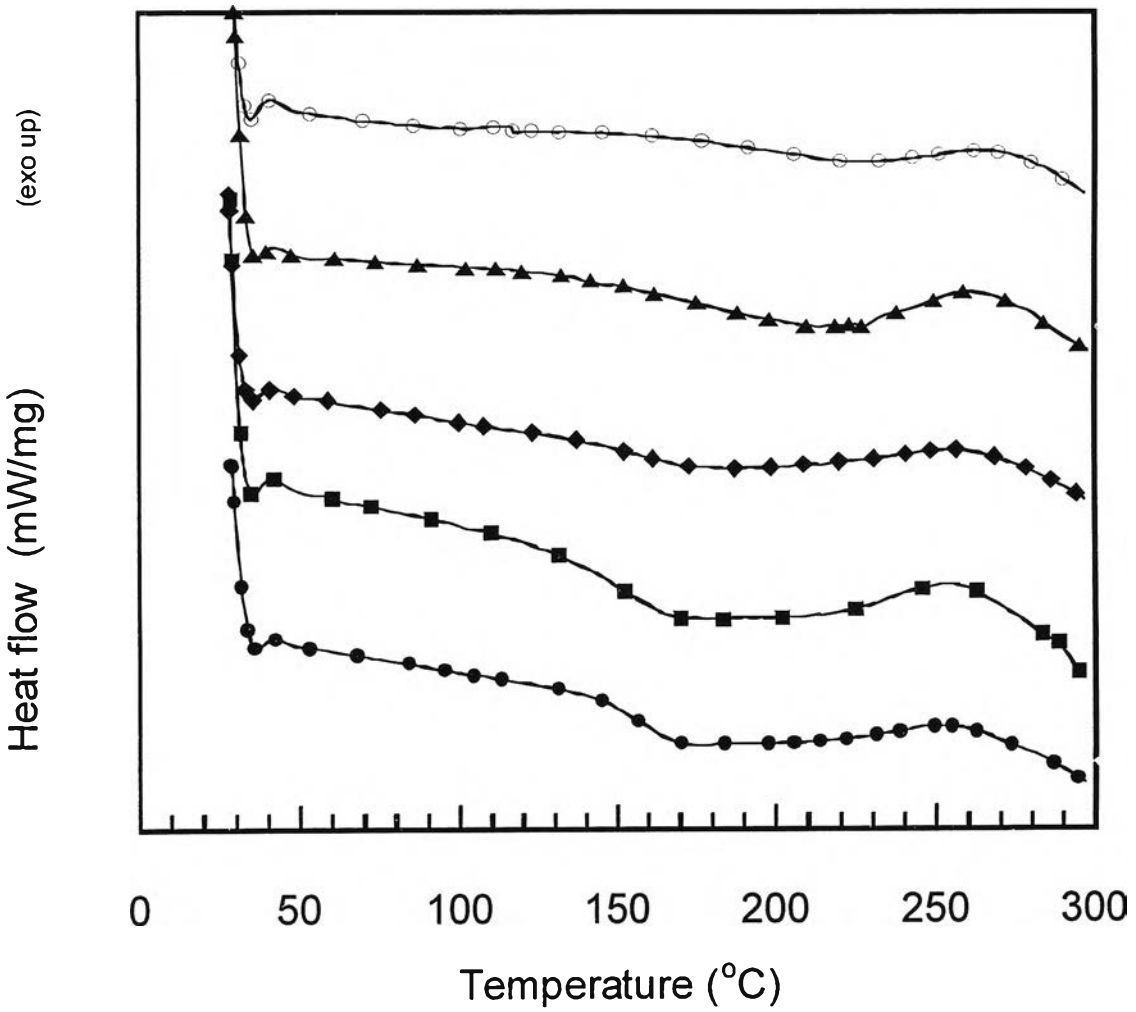

Figure 5.5: DSC thermograms of the fully BA/PU polymer alloys at various compositions: (●) 100/0, (■) 90/10, (◆) 80/20, (▲) 70/30, (○) 60/40

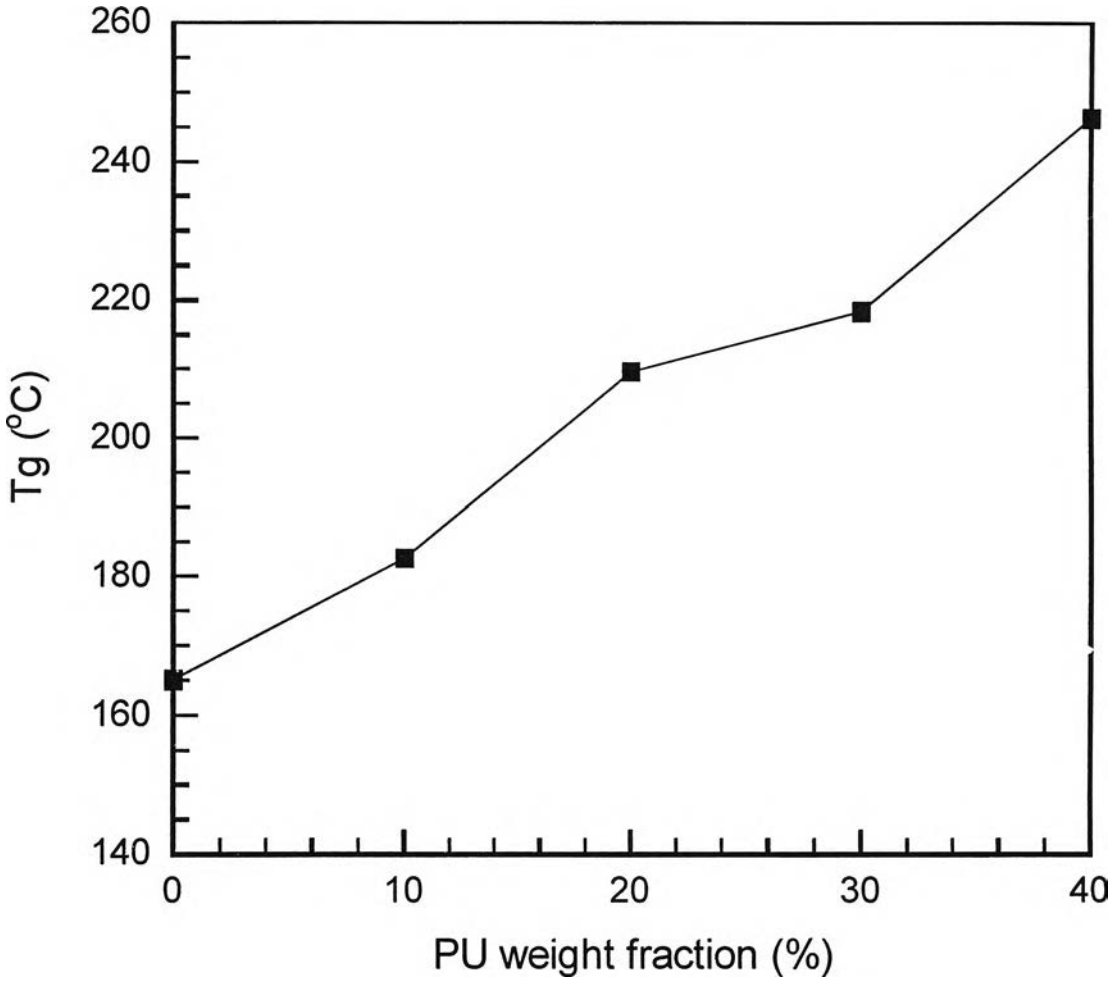

Figure 5.6: Relation between urethane content and glass transition temperature from DSC of the BA/PU alloys.

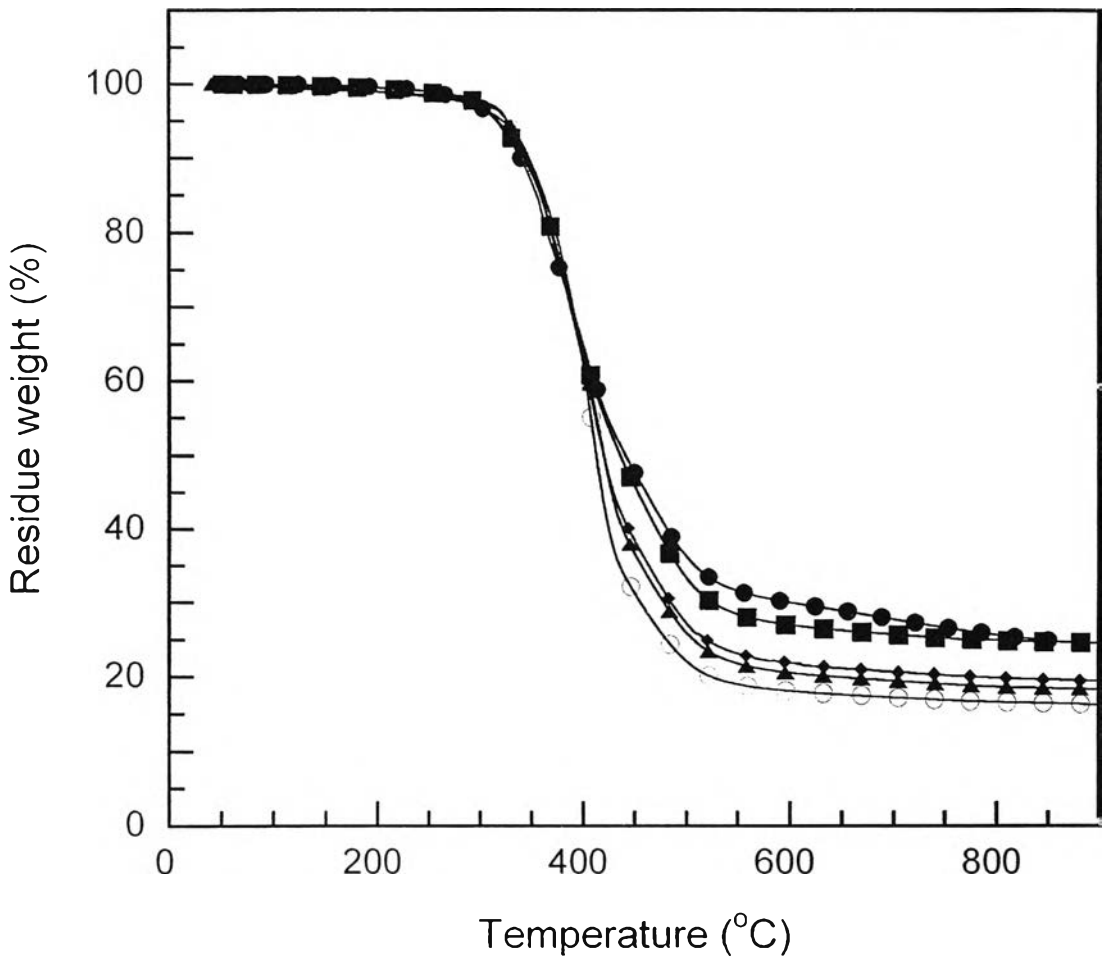

Figure 5.7: TGA thermograms of the BA/PU polymer alloys at various compositions: (●) 100/0, (■) 90/10, (◆) 80/20, (▲) 70/30, (○) 60/40

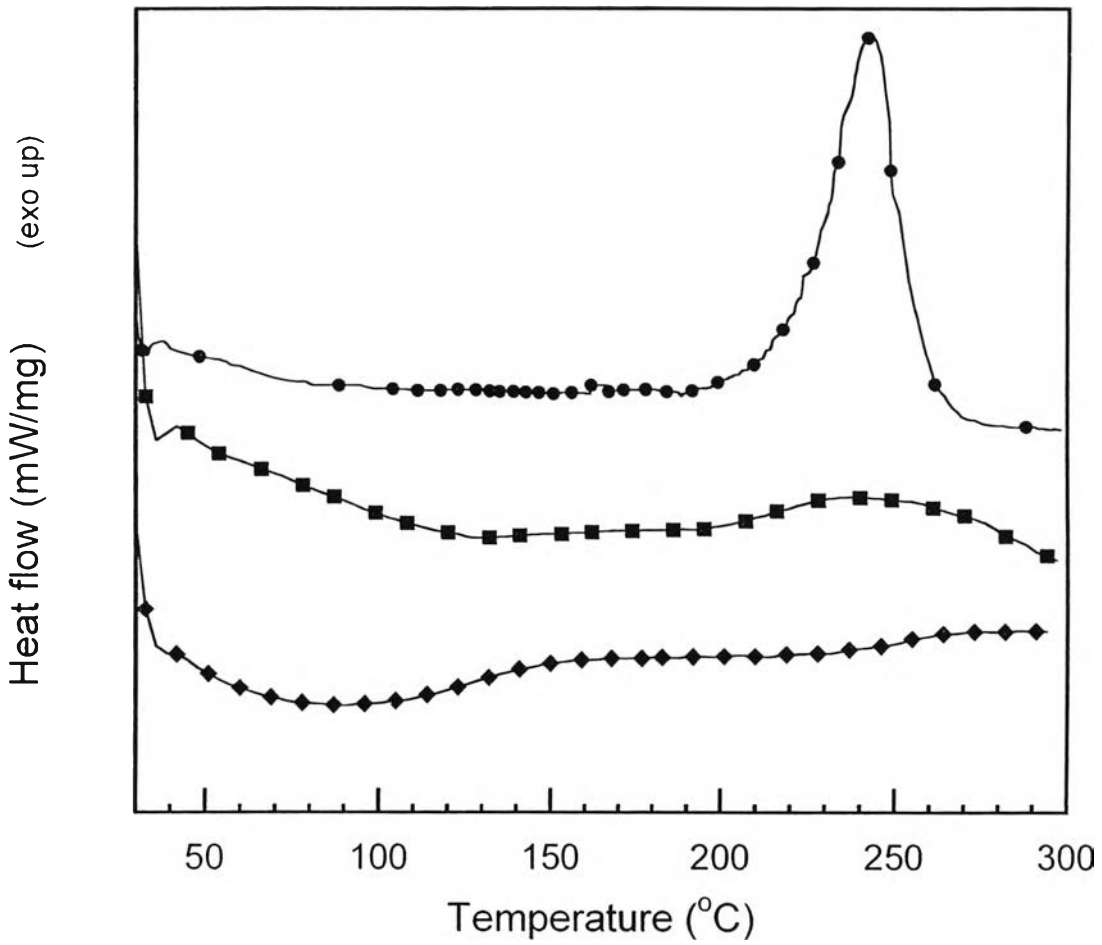

Figure 5.8: DSC thermograms of the Kevlar™-reinforced BA/PU at mass ratio of 60/40 using various curing conditions: (●) uncured, (■) 160°C/2h, and 180°C/2h, (◆) 160°C/2h, 180°C/2h, and 200°C/2h

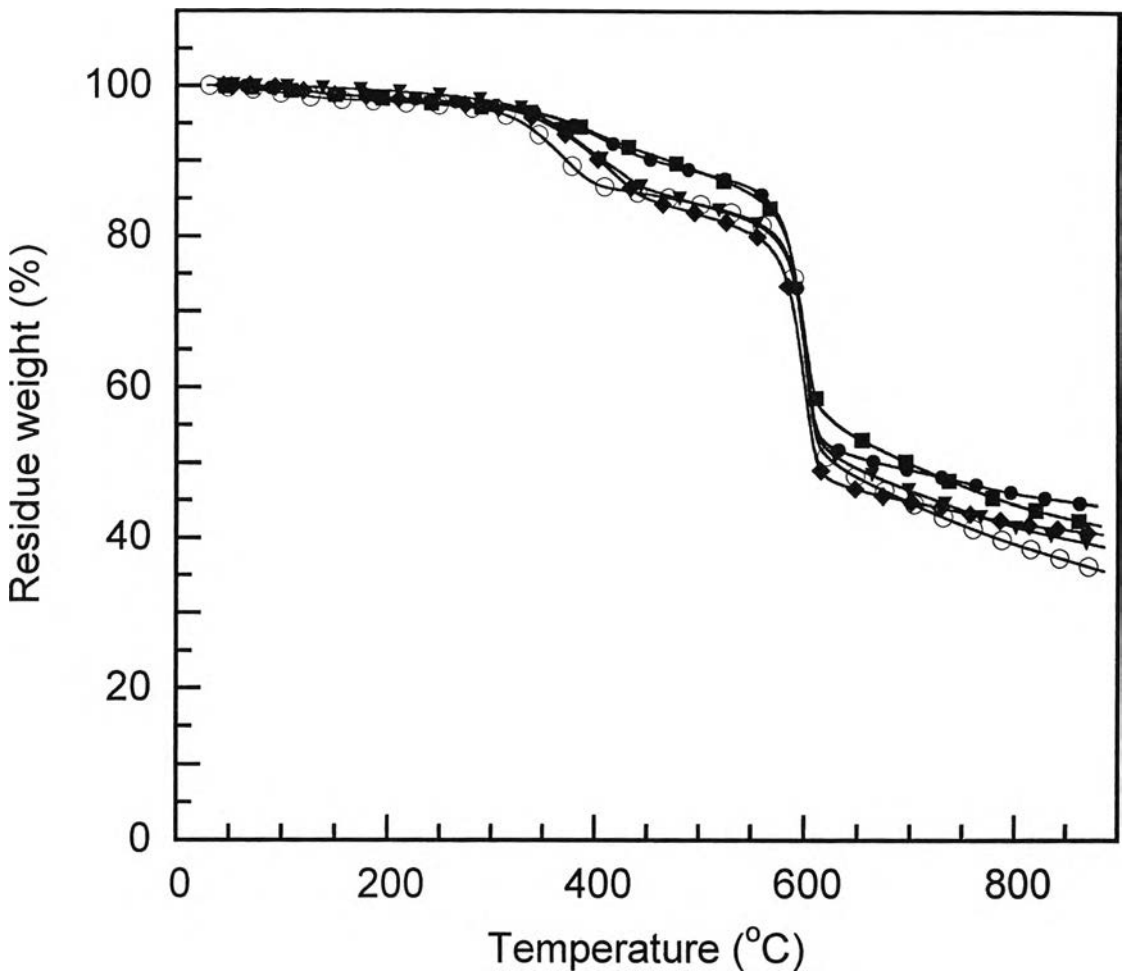

Figure 5.9: Thermal degradation behaviors of the Kevlar™-reinforced BA/PU alloys at various compositions: (●) 100/0, (■) 90/10, (◆) 80/20, (▲) 70/30, (○) 60/40

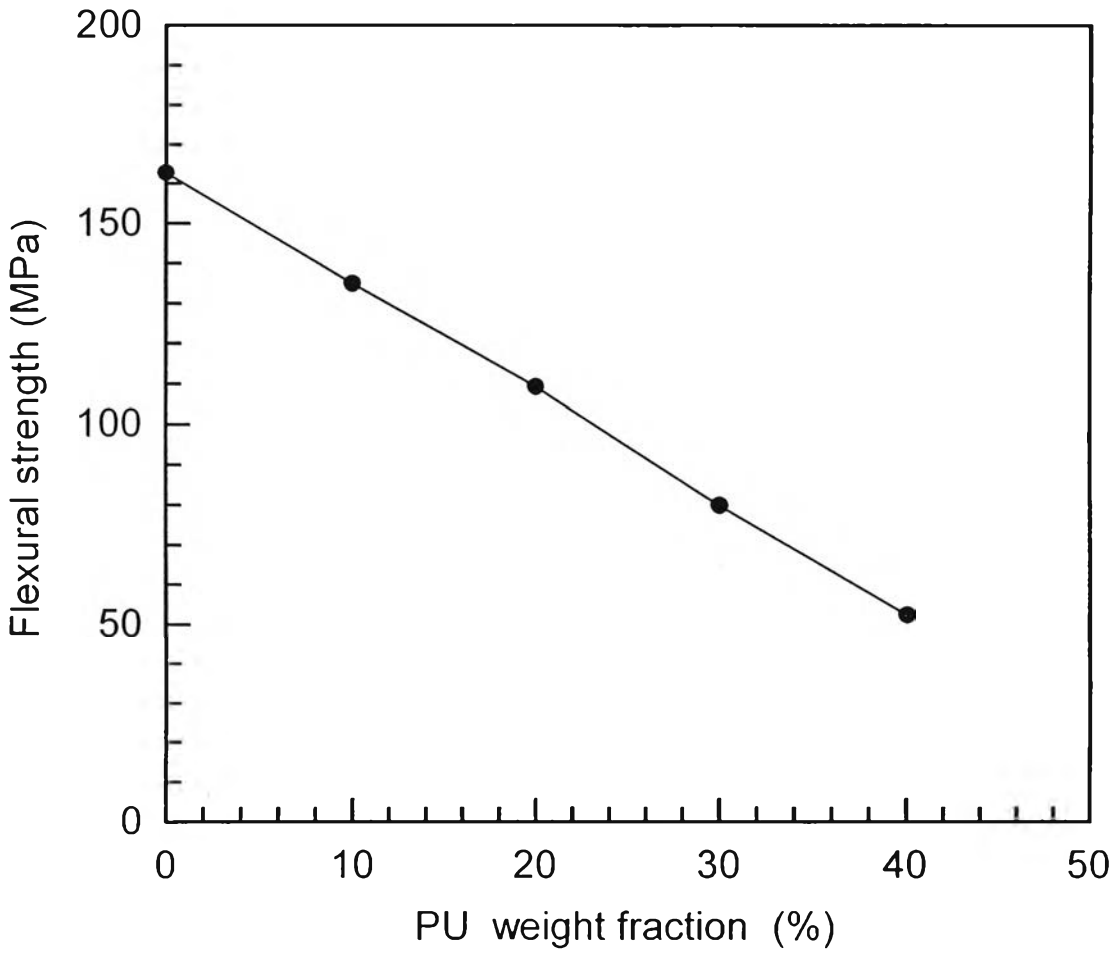

Figure 5.10: Relation between flexural strength and urethane content of the Kevlar^{TM}-reinforced BA/PU alloys

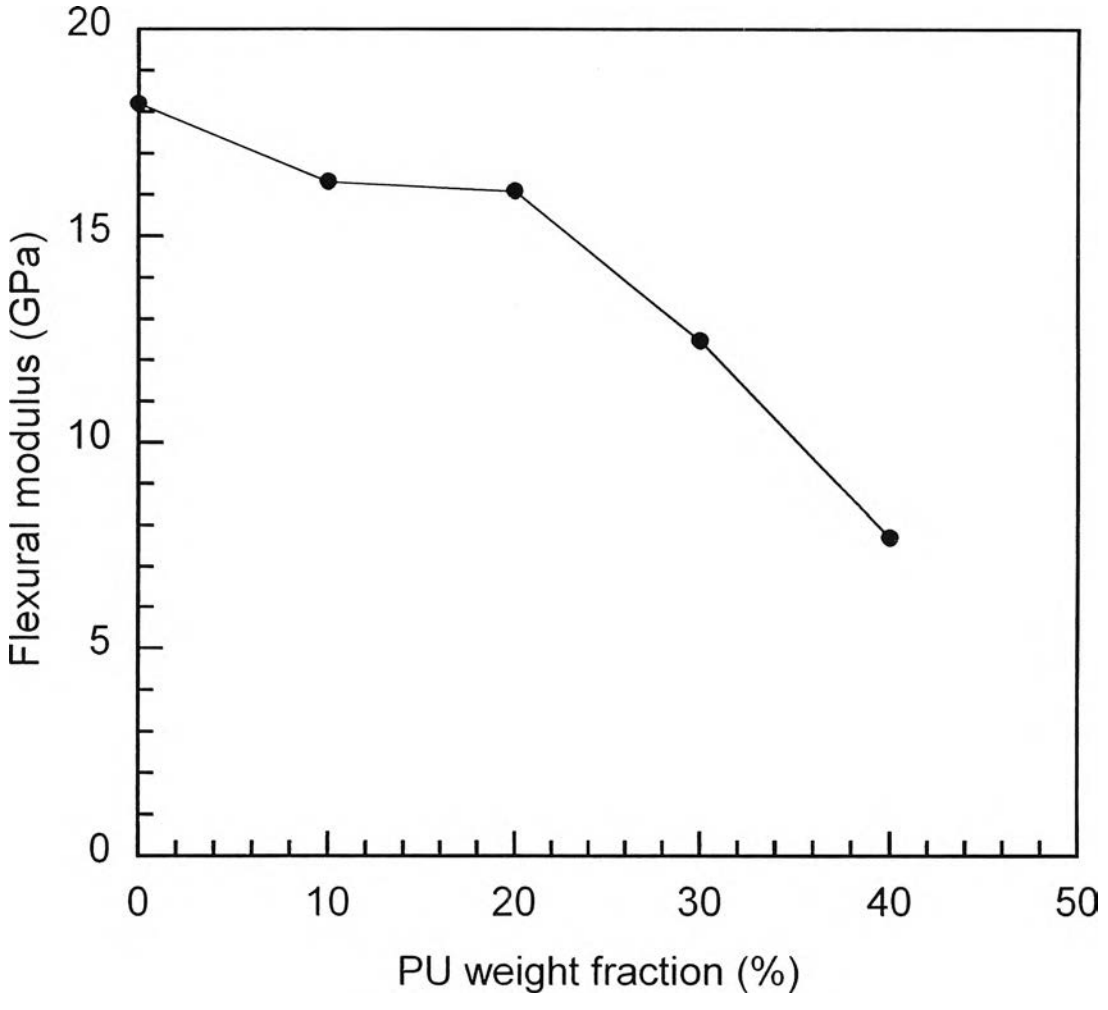

Figure 5.11: Relation between flexural modulus and urethane content of the Kevlar^{TM}-reinforced BA/PU alloys

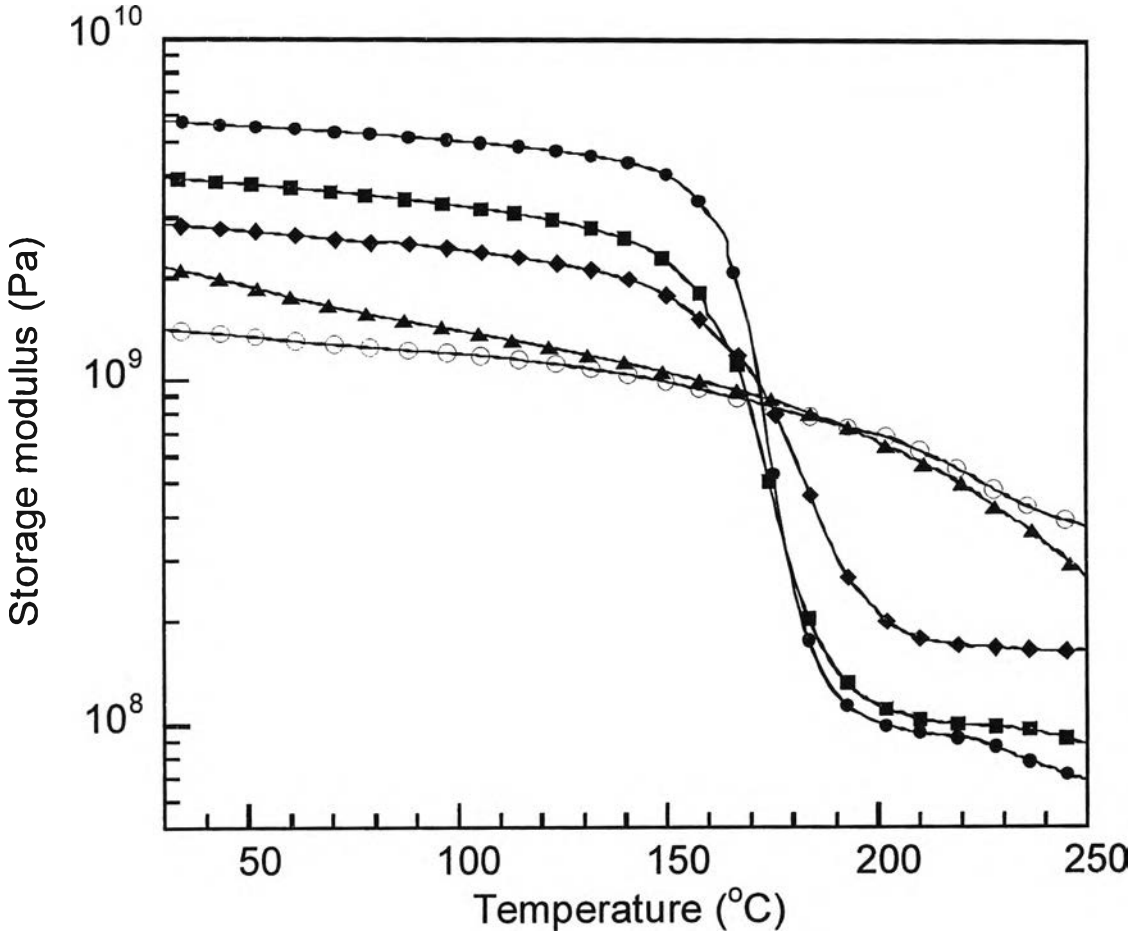

Figure 5.12: Stroage moduli of BA/PU alloys at various mass ratios:
(●) 100/0, (■) 90/10, (◆) 80/20, (▲) 70/30, (○) 60/40

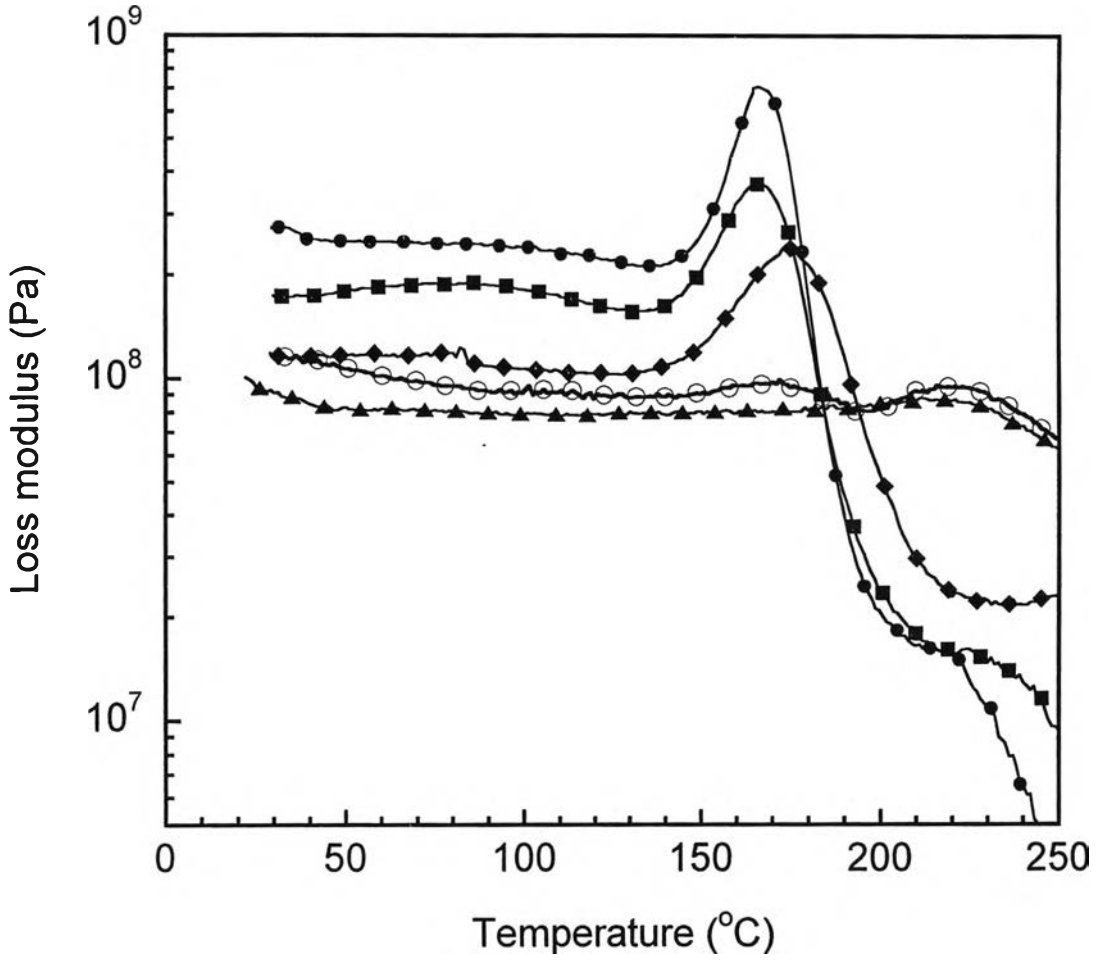

Figure 5.13: Loss moduli of BA/PU alloys at various mass ratios:
(●) 100/0, (■) 90/10, (◆) 80/20, (▲) 70/30, (○) 60/40

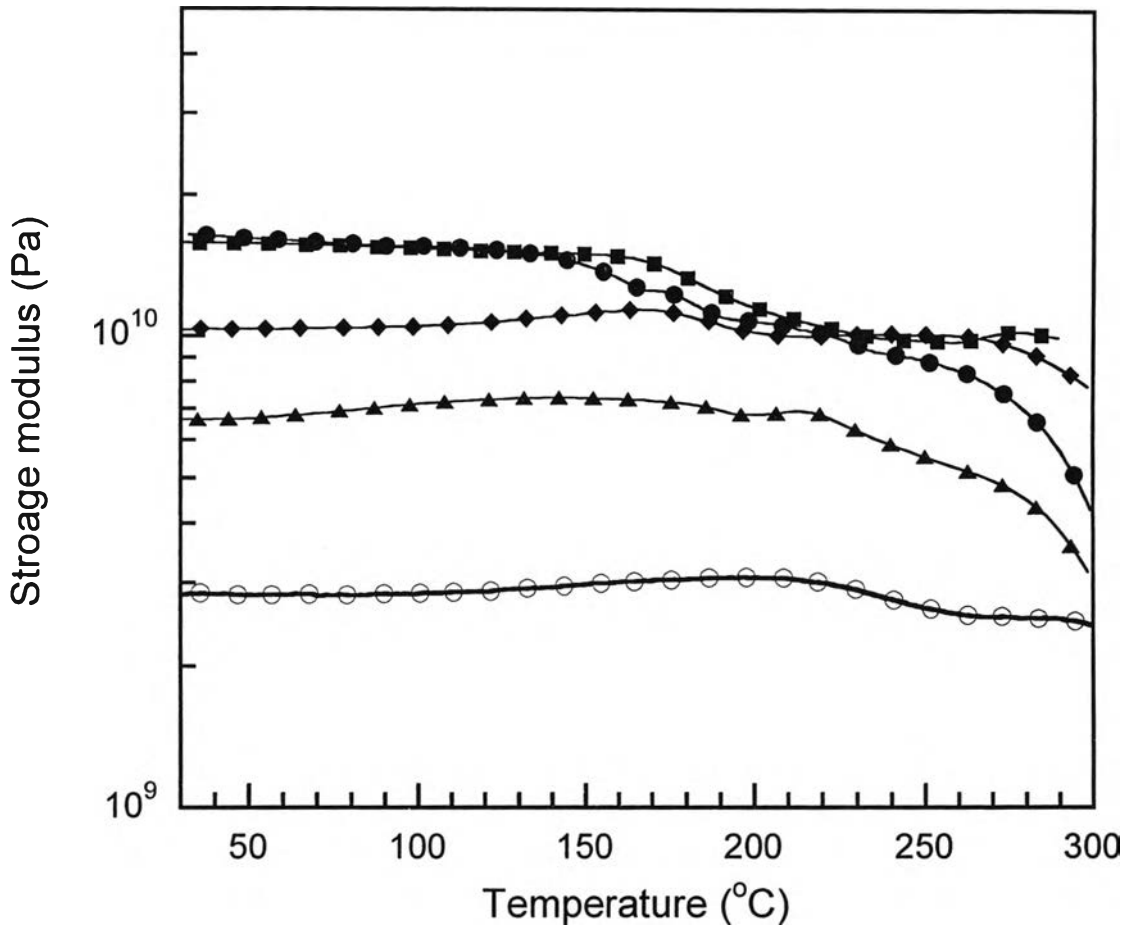

Figure 5.14: Stroage moduli of the Kevlar™-reinforced BA/PU alloys at various mass ratios of BA/PU (●) 100/0, (■) 90/10, (◆) 80/20, (▲) 70/30, (○) 60/40

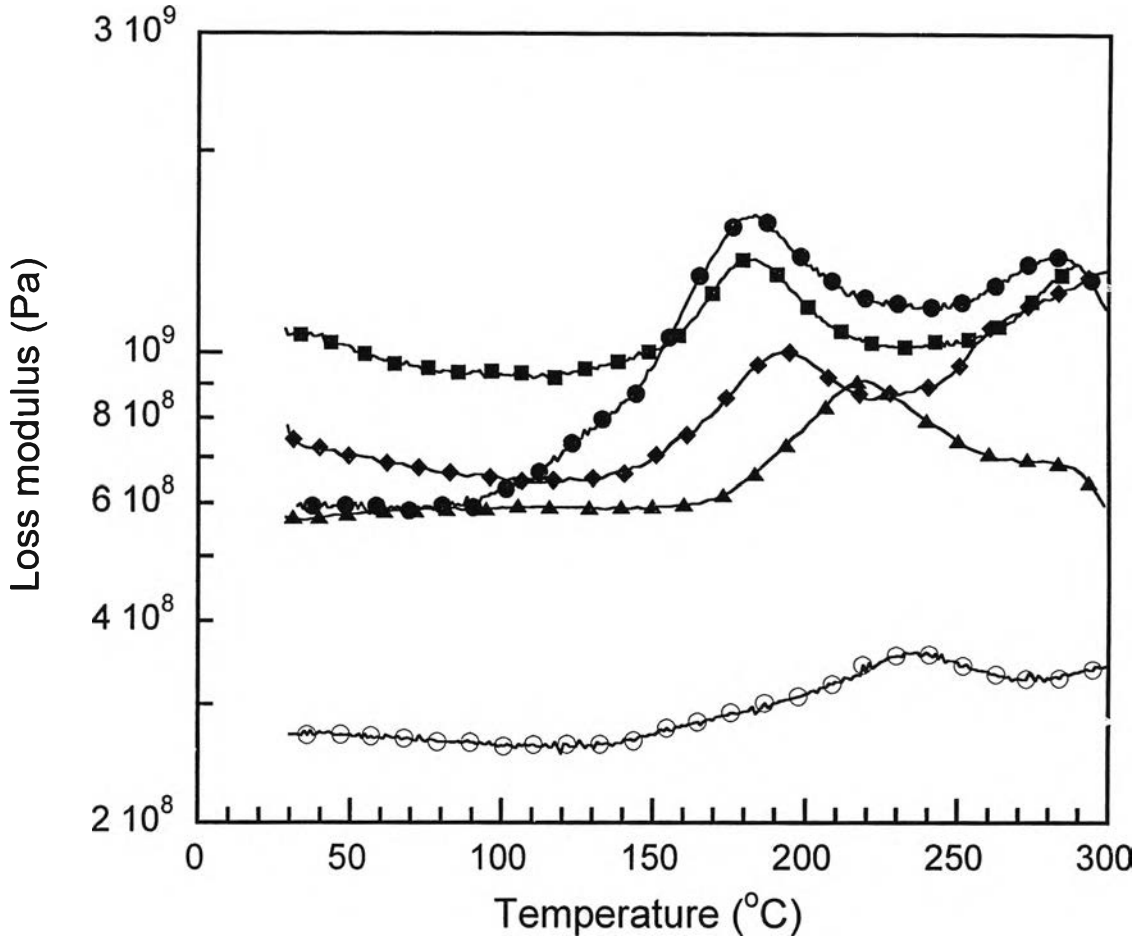

Figure 5.15: Loss moduli of the Kevlar™-reinforced BA/PU alloys at various mass ratios of BA/PU: (●) 100/0, (■) 90/10, (▲) 80/20, (◆) 70/30, (○) 60/40

ต้นฉบับ หน้าขาดหาย

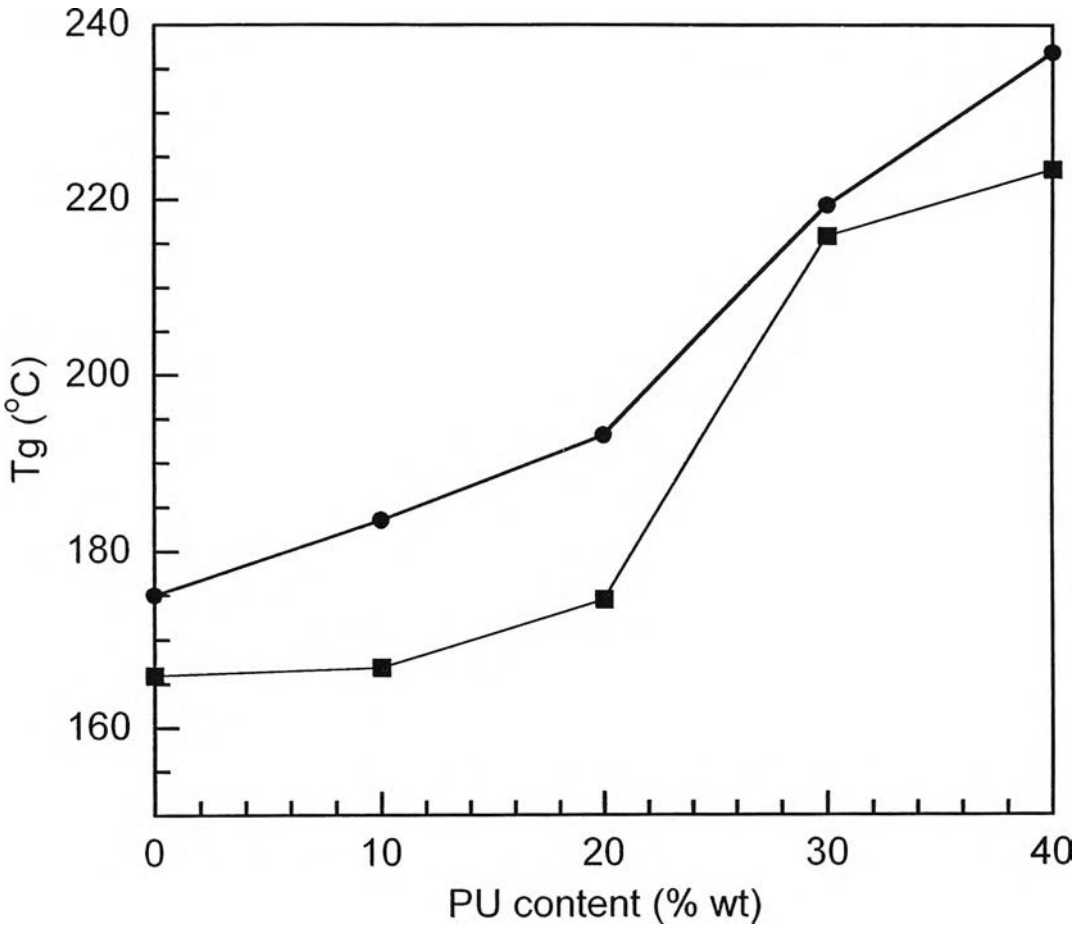

Figure 5.17: Relation between urethane content and glass transition temperature from loss modulus peak: (●) BA/PU alloys, (■) Kevlar^{TM}-reinforced BA/PU alloys

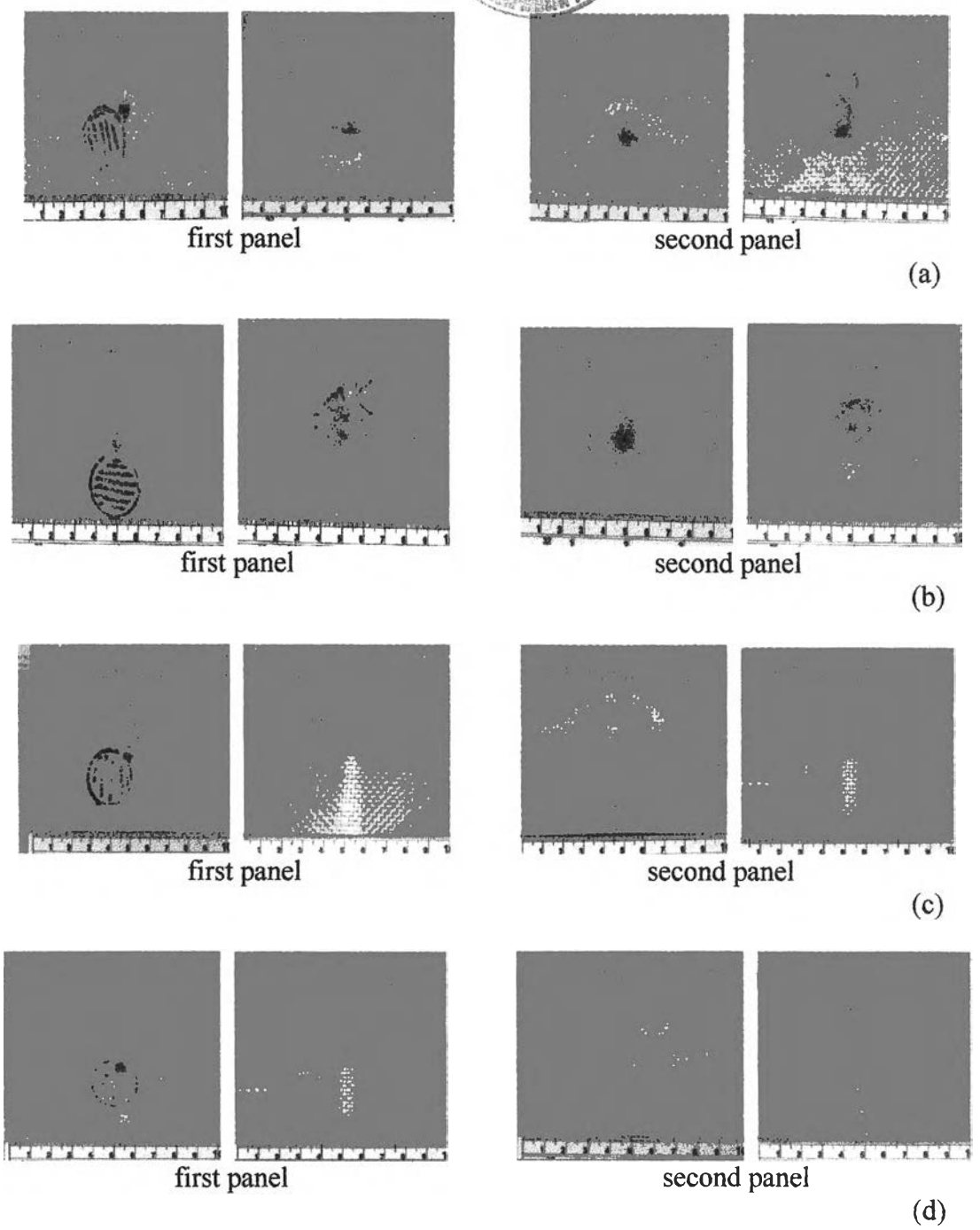

Figure 5.18: Damaged and delaminated area of 10 piles/panel with the samples arrangment of 10/10 after impact with standard lead projectiles with lead outer-coating typically used in 9 mm (a) Kevlar^{TM}-reinforced epoxy, (b) Kevlar^{TM}-reinforced benzoxazine, (c) Kevlar^{TM}-reinforced 90/10 BA/PU, (d) Kevlar^{TM}-reinforced 80/20 BA/PU

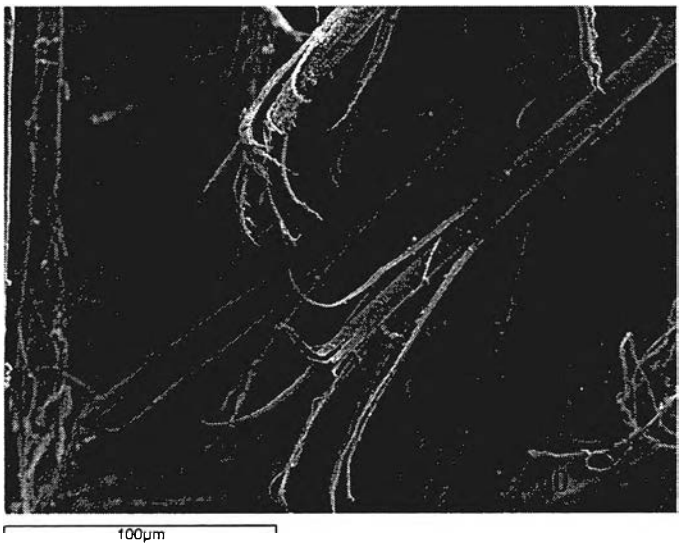

Figure5.19: SEM micrographs of the composite fracture surface showing a deformation of the Kevlar^{TM} fiber after impact with standard lead projectiles

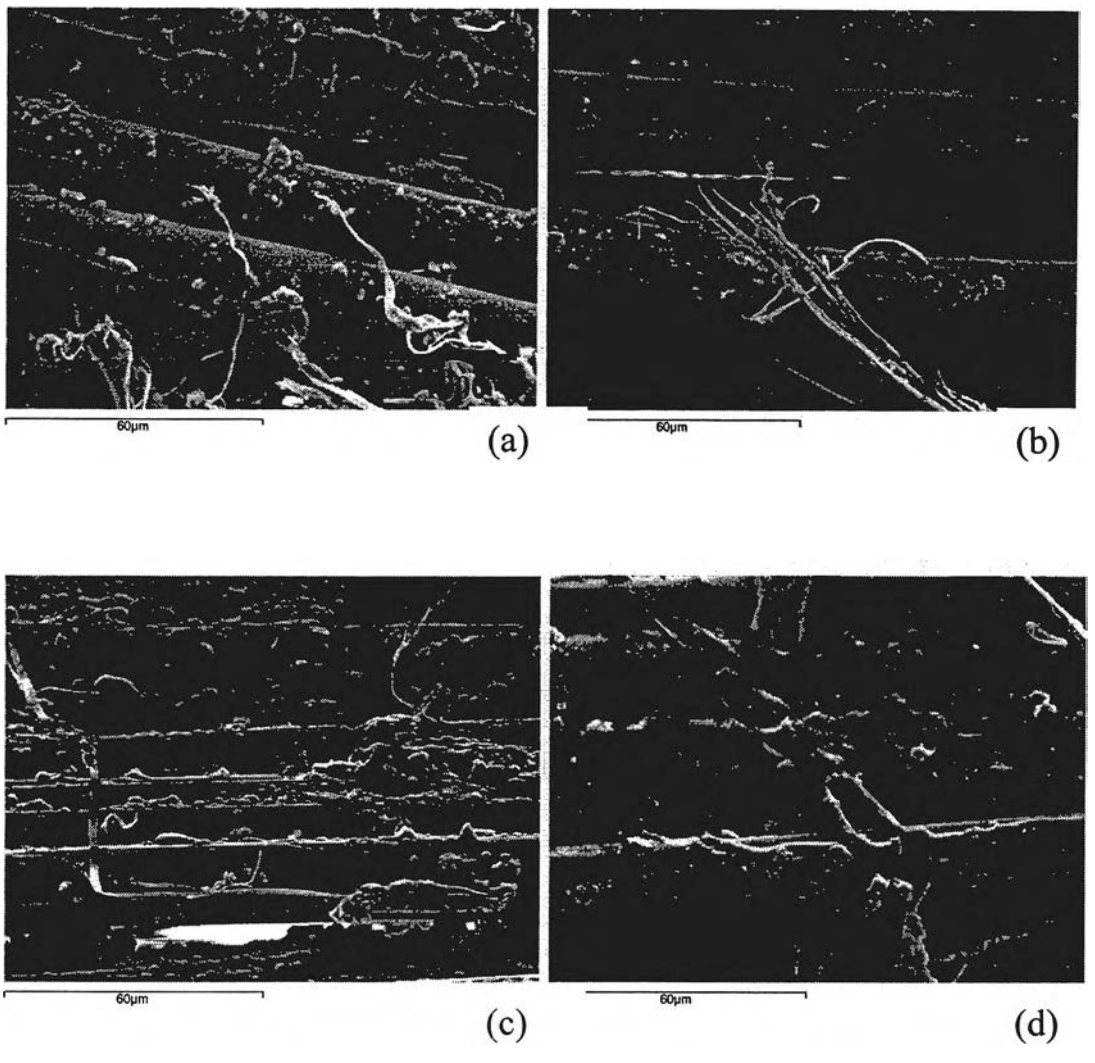

Figure5.20: SEM micrographs of the fracture surface of Kevlar^{TM} reinforced composites after impact with standard lead projectiles : (a) Kevlar^{TM}-reinforced benzoxazine, (b) Kevlar^{TM}-reinforced 80/20 BA/PU, (c) Kevlar^{TM}-reinforced 70/30 BA/PU, (d) Kevlar^{TM}-reinforced 60/40 BA/PU

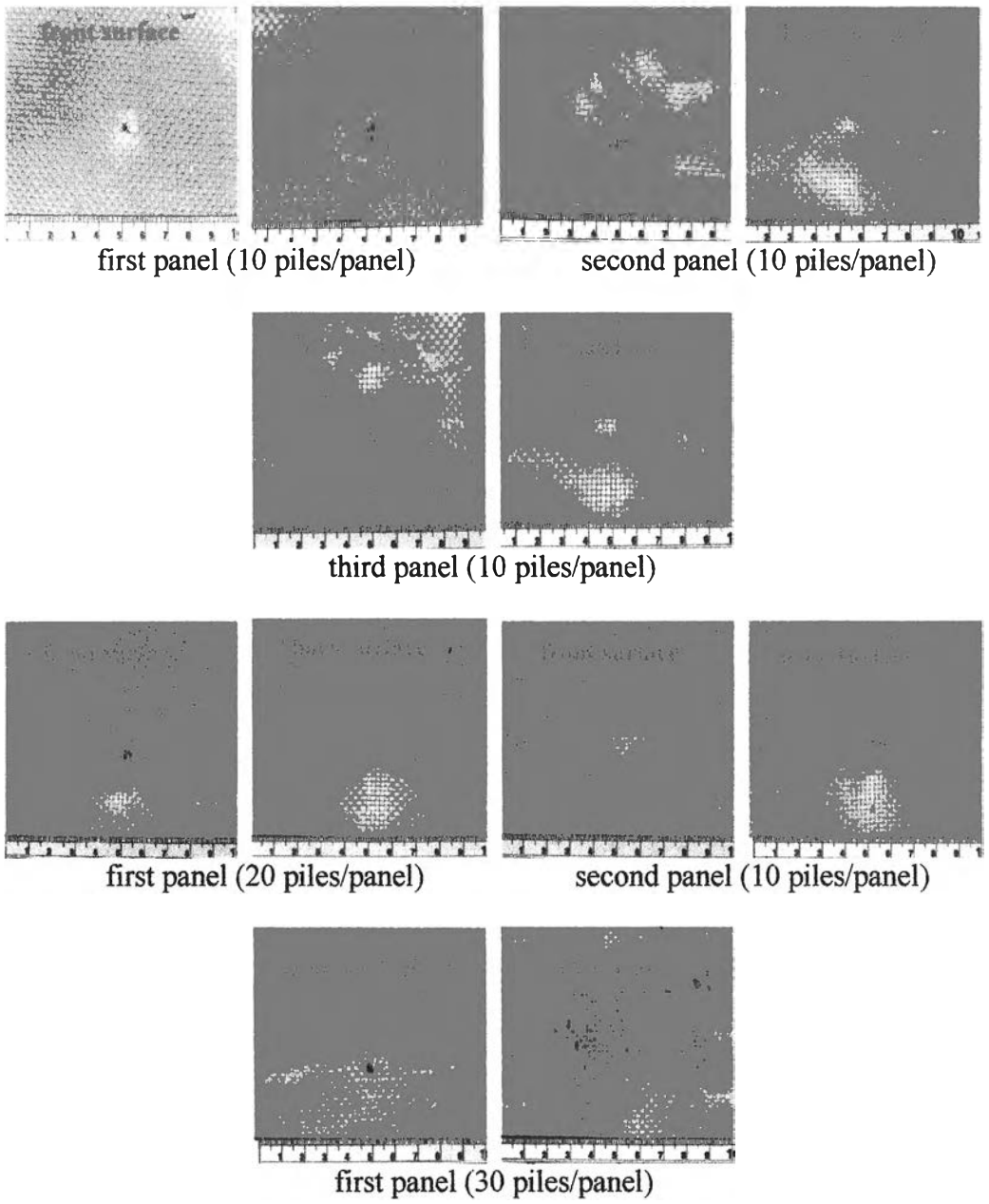

Figure 5.21: Damaged and delaminated area of sample after impact with projectiles velocities which required by NIJ standard for level II-A with the sample arrangement of: (a) 10/10/10, (b) 20/10/0 and (c) 30/0/0

(a)

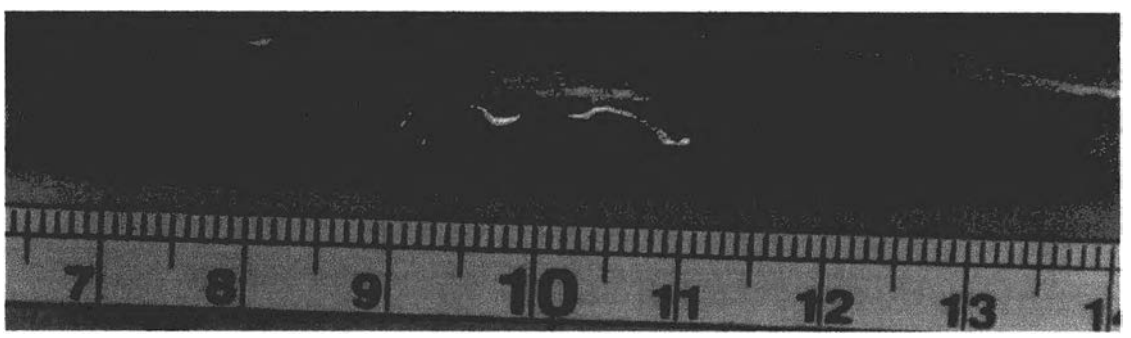

(b)

Figure 5.22: Damaged panel cross-sections of specimen can stop which has stopped projectiles at a velocities required by NIJ standard for level II-A (a) first panel of sample having arrangement of 20/10/0, (b) first panel of sample having arrangement of 30/0/0

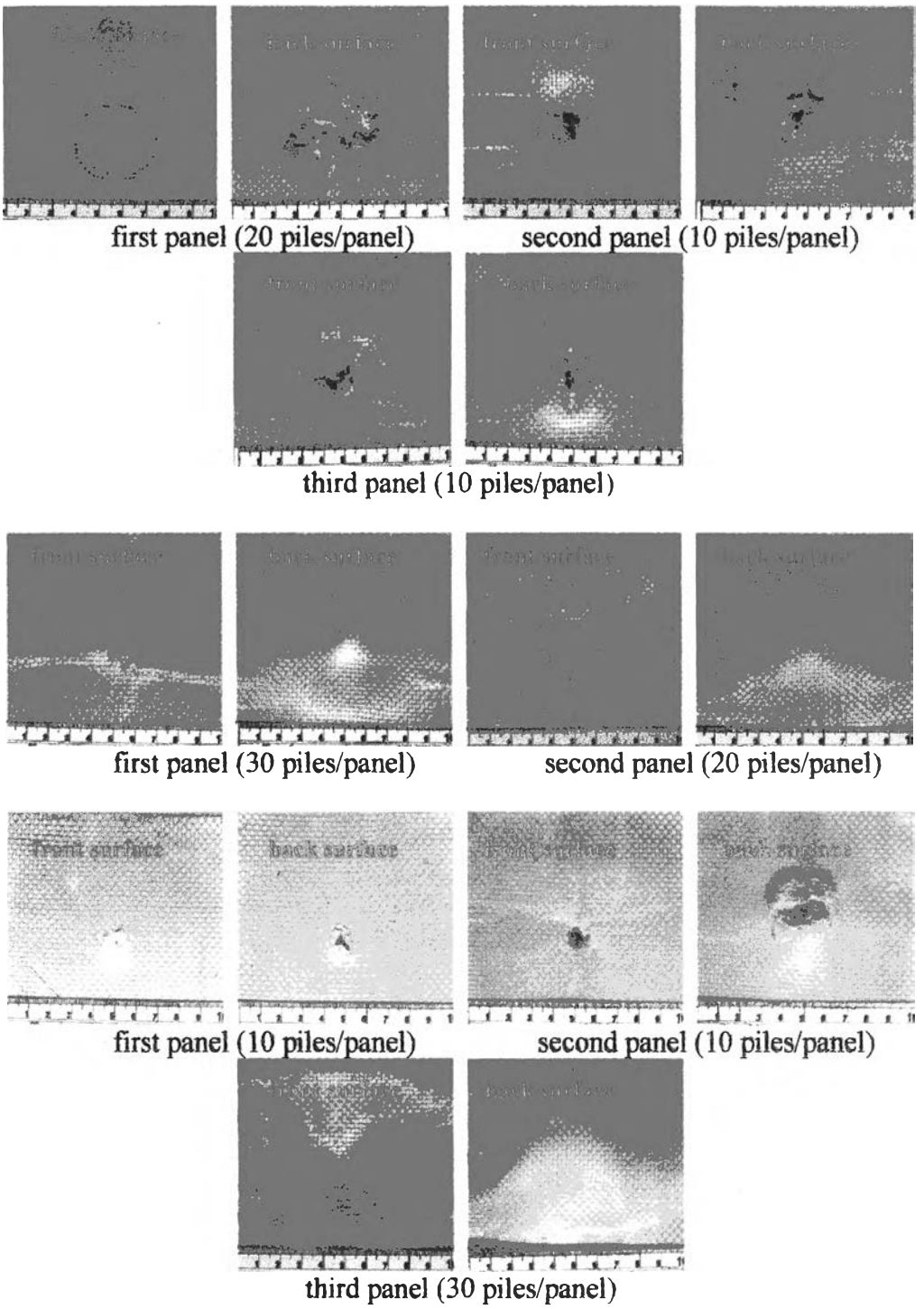

Figure 5.23: Damaged and delaminated area of sample after impact with projectiles velocities which required by NIJ standard for level III-A with the sample arrangement of: (a) 20/10/10, (b) 30/20/0 and (c) 10/10/30

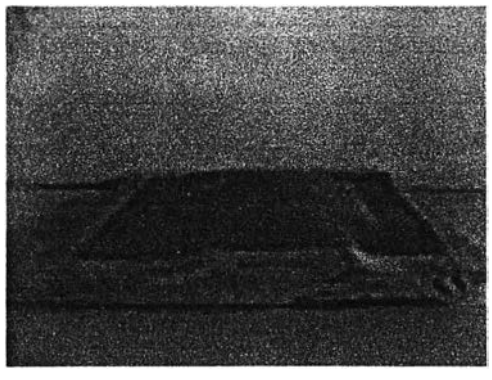

(a)

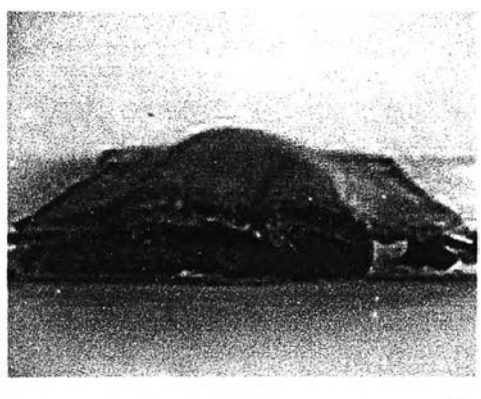

(b)

Figure 5.24: Side view of the samples after impact with projectile velocities which required by NIJ standard for level III-A (a) sample 3b having a configuration of 30/20/0, (b) sample 3c having a configuration of 10/10/30